DLR-IB-RM-OP-2019-140

System Identification and Control Design for a Stratospheric Flight Mission of a Solar Electric Aircraft

Master's Thesis

Arti Kalra

Deutsches Zentrum
für Luft- und Raumfahrt

Institut für Robotik und Mechatronik

BJ.: 2019

DLR-IB-RM-OP-2019-140

MASTERARBEIT

SYSTEM IDENTIFICATION AND CONTROL DESIGN FOR A STRATOSPHERIC FLIGHT MISSION OF A SOLAR ELECTRIC AIRCRAFT

Freigabe:	Der Bearbeiter:	Unterschriften
	Arti Kalra	Arti Kalra
	Betreuer:	
	Tin Muskardin	
	Der Institutsdirektor	
	Dr. Alin Albu-Schäffer	

Dieser Bericht enthält 79 Seiten, 40 Abbildungen und 20 Tabellen

Ort: Oberpfaffenhofen	Datum: 27.09.2019	Bearbeiter: Arti Kalra	Zeichen:

Master of Science in Aerospace Engineering

Major: Aerospace Systems and Controls

Masters Thesis

SYSTEM IDENTIFICATION AND CONTROL DESIGN FOR A STRATOSPHERIC FLIGHT MISSION OF A SOLAR ELECTRIC AIRCRAFT

Supervised by:

Tin MUSKARDIN (DLR)

Valerie BUDINGER (ISAE SUPAERO)

Author:

Arti KALRA

DECLARATION BY STUDENT

This thesis report is entirely my own work and written in my own words. Quotations from literature are properly indicated with appropriated references in the text. All literature used in this piece of work is indicated in the bibliography placed at the end. I confirm that no sources have been used other than those stated.

I understand that plagiarism (copy without mentioning the reference) is a serious examinations offence that may result in disciplinary action being taken.

Author **Arti KALRA**

Date: .... Signature: ....

Acknowledgements

I am grateful to God for having helped me in all moments. Without Him nothing would have been possible.

I would like to thank ISAE SUPAERO for having provided me with the means to become an Aerospace System and Controls engineer and DLR for providing me an opportunity to work on this topic for my masters thesis.

Foremost, I would like to express my sincere gratitude towards my Supervisor at DLR, Mr. Tin Muskardin, for his continuous support and guidance during my internship. I'm grateful to him for being always very interested into the progress of the tasks and willingness to teach and help.

I would also like to express my gratitude to my supervisor and professor at ISAE SUPAERO Mrs. Valerie Bundiger and Mr. Yves Briere for for teaching me the way of thinking and solving problems in the courses I had with them.

I have to thank warmly all my colleagues specially Raja Judeh, Patrick Krömer and Eduardo Rodrigues Della Noce for all the useful technical discussions in connection with the topic in the office.

I am especially grateful to my family for all love and support. For providing me with a home where I could grow personally and professionally.

List of Figures

1.1 Elektra Solar Two OPS in flight [1] 3

2.1 Steps of System Identification Process 6

3.1 Stability margins in a Step Response [2] 22
3.2 Distribution of Crosswind 24
3.3 Distribution of Tailwind 24

4.1 Measured longitudinal and lateral states and states generated from the integration of the 6DOF equations of motion with corrected accelerations: Identification Set 26
4.2 Measured longitudinal and lateral states and states generated from the integration of the 6DOF equations of motion with estimated biases added: Identification Set 27
4.3 Reconstructed forces and moments, and forces and moments from linear regression: Identification set 29
4.4 Measured longitudinal and lateral states and states generated from the integration of the 6DOF equations of motion with corrected accelerations: Validation Set . 31
4.5 Measured longitudinal and lateral states and states generated from the integration of the 6DOF equations of motion with estimated biases added: Validation Set . 32
4.6 Reconstructed forces and moments, and forces and moments from linear regression: Validation Set 33
4.7 Validation of Estimated model using aircraft equations of motion: Identification Set 35
4.8 Validation of Estimated model using aircraft equations of motion: Validation Set 36
4.9 Response for Airspeed 37
4.10 Response for Altitude 37
4.11 Response for course angle 37
4.12 Bode Diagram for the system with Initial Control Design 38
4.13 Bode Diagram for the system with Optimization-based Control Design 38

4.14 Step response for airspeed with Initial Control Design 39
4.15 Step response for airspeed with Optimization-based Control Design 39
4.16 Distribution of Crosswind 40
4.17 Distribution of Tailwind 40
4.18 Airspeed output from a Monte Carlo experiment with gust disturbance 41
4.19 Overshoot in Airspeed 41
4.20 Undershoot in Airspeed 41
4.21 Altitude output from a Monte Carlo experiment with gust disturbance 42
4.22 Overshoot in Altitude 42
4.23 Undershoot in Altitude 42
4.24 Airspeed output from a Monte Carlo experiment with gust disturbance and model parameter variations 43
4.25 Overshoot in Airspeed 43
4.26 Undershoot in Airspeed 43
4.27 Altitude output from a Monte Carlo experiment with gust disturbance and model parameter variations 44
4.28 Overshoot in Altitude 44
4.29 Undershoot in Altitude 44

A.1 Measured longitudinal and lateral states and states generated from the integration of the 6DOF equations of motion with estimated biases added: Identification Set 53
A.2 Reconstructed forces and moments, and forces and moments from linear regression: Identification set 54

B.1 Lateral Autopilot Design [3] 56
B.2 Pitch angle inner loop [3] 57
B.3 Thrust inner loop [3] 58
B.4 Longitudinal Autopilot Design [3] 59

List of Tables

2.1 Characteristics of Validation metrics 17

4.1 Orientation of IMU sensor w.r.t. body axes 26

4.2 Estimated measurement biases for each maneuver 28

4.3 Values of longitudinal force and moment derivatives using linear regression . . 29

4.4 Statistical measures of the reconstructed states using flight path reconstruction: Identification Set 30

4.5 Statistical measures of the longitudinal force and moments using Two step method: Identification Set 30

4.6 Orientation of IMU sensor w.r.t. body axes: Validation Set 31

4.7 Estimated measurement biases for each maneuver: Validation Set 32

4.8 Statistical measures of the reconstructed states: Validation Set 32

4.9 Statistical measures of the longitudinal force and moments using Two step method: Validation Set 34

4.10 Statistical measures of the states obtained using Two step method: Identification Set 35

4.11 Statistical measures of the states obtained using Two step method: Validation Set 35

A.1 Designing the Input 49

A.2 Steps for Data Extraction and Pre-processing 50

A.3 Steps of the Two Step Method and Validation of the Model 50

A.4 Orientation of IMU sensor w.r.t. body axes 53

A.5 Estimated measurement biases for each maneuver 54

A.6 Statistical measures of the reconstructed states using flight path reconstruction: Identification Set 55

A.7 Statistical measures of the longitudinal force and moments using Two step method: Identification Set 55

A.8 Statistical measures of the states obtained using Two step method: Identification Set 55

Abstract

A system identification approach is presented for Elektra Two Solar OPS, a high altitude long endurance (HALE) aircraft for stratospheric flight missions. A linear longitudinal model of the aircraft has been developed using a Two Step Method based system identification approach, which provides the biases in the states in the first step along with the force and moment parameters of a system in the second step unlike other common system identification approaches. In order to prove the credibility of the identified aircraft longitudinal model, the identified model has been validated using various methods including some statistical measures, a validation set from the flight test recorded data and a forward simulation to compute the states from the identified model.

An optimization based controller tuning method has been presented based on a control design which was manually tuned in flight, using Ziegler-Nichols method which is not a reliable method for such stratospheric flight missions. The applicability of the designed controller has been verified using various methods. A frequency and time domain analysis has been performed to analyse the stability margins and compare other characteristics. A robustness analysis has been performed using Monte-Carlo simulations for a gust disturbance and the model parameter variations in order to validate the robust behaviour of the designed controller. Extensive simulation studies demonstrate that the proposed approach is capable of achieving a an acceptable model of the aircraft which is suitable to be used for the ultimate goal of autonomous stratospheric flight.

Keywords: System identification, Two Step Method, HALE, Optimization based Control Design

Symbols

u, v, w	Linear velocities along the body fixed x, y and z axes
a_x, a_y, a_z	Linear accelerations along the body fixed x, y and z axes
ψ, θ, ϕ	Roll, pitch and yaw angles
p, q, r	Roll, pitch and yaw rates
X, Y, Z	Longitudinal, lateral and normal forces
L, M, N	Rolling, pitching and yawing moment
h	Aircraft altitude
δ_t, δ_e	Throttle and elevator deflection
$I_x xL, I_y y, I_z z$	Moment of Inertias along x, y and z axes
$X_0, X_u, X_w, X_q, X_{\delta e}, X_{\delta t}$	Longitudinal force derivatives
$Z_0, Z_u, Z_w, Z_q, Z_{\delta e}$	Normal force derivatives
$M_0, M_u, M_w, M_q, M_{\delta e}$	Pitching moment derivatives
t_s	Settling time
OS_{max}	Maximum Overshoot
$\lvert\dot{u}\rvert$	Maximum rate of change of control command

About DLR

The Deutsches Zentrum für Luft- und Raumfahrt e.V. (the German Aerospace Center), abbreviated DLR, is the national research center for Aerospace, Energy and Transportation sectors in Germany. The headquarters of DLR are located in Cologne and is present in 20 additional sites in Germany and a few more locations out of Germany (Paris, Brussels and Washington). A wide range of research and development projects in national and international partnerships are being carried out by DLR. The research for various types of robots is conducted at Oberpfaffenhofen near Munich, in the Institute of Robotics and Mechatronics. The Institute of Robotics and Mechatronics develops a wide array of robots for enormous applications.The institute headed by Prof. Dr.-Ing. Alin Olimpiu Albu-Schäffer intends to develop a variety of robots which perform several tasks of locomotion and interaction with the environment with a wide range of autonomy. The institute has various departments and research groups. The research is carried out in the following groups, 3D perception, legged robots, bionics, flying robots, medical robots, compliant robotics systems, telepresence and VR. I was a part of the flying robots group.

Flying Robots

The group mainly carries research in the following domains, aerial manipulation, high altitude platforms, landing on mobile platforms, Takeoff and Landing of VTOL UAVs on a Moving Platform, Vision Guided Navigation of UAVs, Mission Planning and Validation and unmanned airships. The research group is headed by Dr. Ing. Konstantin Kondak. I was working in the high altitude platforms domain. High-altitude platforms are capable of extending application fields presently covered by satellites and are therefore often named HAPS, which stands for high-altitude pseudo satellites. The DLR Flying Robots group is working in close cooperation with Elektra Solar GmbH on highly efficient drives, avionics components, as well as payloads and autonomy functionalities for solar high-altitude platforms. The research in this domain is performed by Tin Muskardin, who was also my supervisor during my internship.

Contents

List of Figures

List of Tables

Abstract

Symbols

About DLR

1 Introduction and Background 1

1.1 Background and Motivation 1

1.2 Objectives and Scope 2

1.3 Elektra 2 2

1.4 Applications 4

1.5 Outline of the thesis 4

2 Aircraft System Identification for Elektra 2 5

2.1 Data Extraction and Pre-Processing 6

2.1.1 Importing the data 7

2.1.2 Processing of data 7

2.1.3 Corrections 8

2.2 Two Step Method 9

2.2.1 Flight Dynamic Model 9

2.2.2 Identification of Orientation of IMU Sensor 11

2.2.3 Flight Path Reconstruction 13

2.2.4 Aerodynamic Model Identification 15

2.3 Model Validation 16

2.3.1 Metrics 16
2.3.2 Forward Simulation for State-Level Validation 17
2.3.3 Validation Set 18

3 Control Design 19
3.1 Initial Control Design 19
3.2 Optimization based Controller Tuning 20
3.3 Stability of the Control System 21
3.4 Robustness Analysis 23
3.4.1 Effect of Wind Gust 23
3.4.2 Monte Carlo Simulations for Parametric Variations 24

4 Results and Observations 25
4.1 System Identification 25
4.1.1 Identification of Orientation of IMU sensor 25
4.1.2 Flight Path Reconstruction Results 26
4.1.3 Aerodynamic Model Identification 27
4.2 Validation 29
4.2.1 Statistical Metrics 29
4.2.2 Validation Set 30
4.2.3 Forward Simulation 34
4.3 Control Design 36
4.3.1 Initial Control Design 36
4.3.2 Stability of the Control system 36
4.3.3 Robustness Analysis 39

Conclusions 45

Bibliography 46

A System Identification Toolchain & Application to Elektra 1 49
A.1 Toolchain 49
A.2 Elektra 1 53

B Fundamental Control Design 56
B.1 Lateral Control Design 56

B.2 Longitudinal Control Design 57
B.3 TECS 58

Chapter 1

Introduction and Background

1.1 Background and Motivation

High Altitude and Long Endurance (HALE) aerial vehicles are getting recognized for having the capabilities to extend the application fields covered by satellites. The present study is based on such a High Altitude, Long Endurance (HALE) aircraft, 'Elektra Two' which is built by the German Aerospace Center (DLR) Spin-Off company Elektra Solar. The main task is to develop simulation models and flight control functionalities for an autonomous stratospheric flight mission. At the moment, the aircraft is capable of autonomous takeoff, trajectory following and landing at low altitude. Currently, only lower altitude flights have been performed which limits the scope of the study. But continuous attempts are being made for further flights with increased altitudes. The idea is to iteratively increase the altitude in steps and reach a final altitude of 20km.

Several attempts have been made for developing high fidelity models for fixed wing HALE UAVs like Elektra1 and Penguin BE UAV for landing applications on a platform mounted on the top of a ground vehicle. In particular, cooperative landings and model based control for landing on moving platforms [4],[5] are leading achievements for research on HALE platforms.

The objectives not only include the development of a valid model but also analysing a control design. The initial flight controller was pre-tuned in simulation using geometry-based aerodynamic models, but manual fine-tuning in flight was still necessary, due to the lack of more accurate models. A reliable simulation model of the aircraft would accelerate the process of developing advanced control strategies to conduct the stratospheric flight mission with actual HALE UAVs.

1.2 Objectives and Scope

The main objective of this research is to implement a system identification approach in order to avoid the need of in-flight manual tuning of the flight control parameters due to lack of more accurate models and reduce the dependency on the geometry based aerodynamic models. The structure obtained should be tested with real flight data, yielding a valid dynamic model of the aircraft suitable for the control design. The second main objective was to implement a control design for an autonomous stratospheric flight with increased stability and robust performance.

Various methods for system modelling, model validation and control of the given flight platforms are to be investigated and implemented. As a first step the system is modelled using a Two Step identiifcation approach. Once the model has been identified, it is very important to validate the accuracy and the reliability of the identified model. In a second step, a suitable optimization based flight control design is implemented for the planned application of the stratospheric mission. The robustness of the control design is to be checked using various methods. A frequency domain analysis and a robustness analysis is to be performed in order to check the credibility of the designed controller.

1.3 Elektra 2

Elektra Two [1], equipped with two seats, is a solar electric high endurance aircraft designed by Elektra Solar GmbH to endure long distances as well as high altitudes. The two-seat tandem solar aircraft uses only the energy from the sun to fly. At lower altitudes, the aircraft can fly with only about 2 kW power whereas the maximum power provided from the sun is about 5 kW. In this case, very long-range and high-altitude flights are achievable. The best guarantee for a safe flight is the complete redundant power unit system for Elektra 2.

The main characteristic of the Elektra 2 is the combination of high glide ratio (over 40) and its light weight. Apart from these characteristics, the other geometric parameters of the OPS (Optional Pilot System) version are : MTOW=486kg, wing span b= 24.8 m and wing area S=27 m^2. Optionally, the aircraft can be flown with a completely autonomous flight system including automatic takeoff and landing because of which it can be classified in the Optional Pilot System (OPS) class. It is also available as Unmanned Autonomous System (UAS) version as it can also fly completely autonomously.

Elektra Two Solar OPS (Optionally Piloted System) was designed to be used as unmanned electric-solar airplane for stratospheric missions at 70.000 ft altitude. The autopilot can be

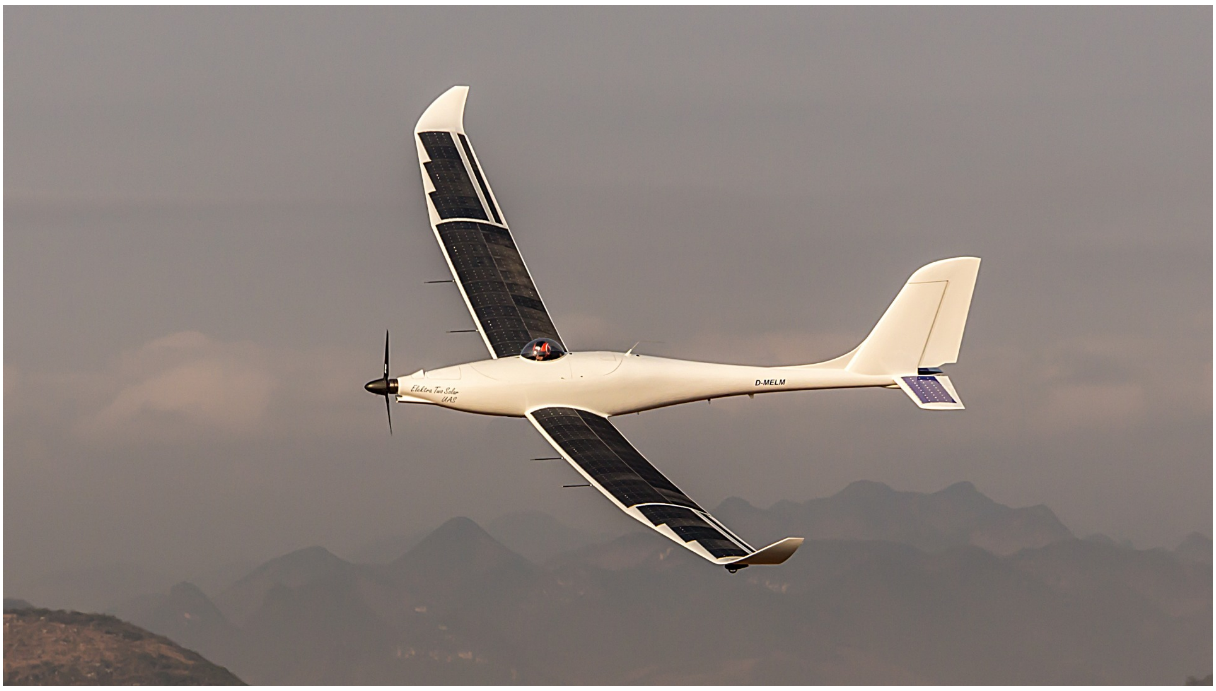

Figure 1.1: Elektra Solar Two OPS in flight [1]

activated or deactivated by the pilot. The power is provided by combined solar and rechargeable batteries. The electrical power unit has double redundancy and consists of two systems working in parallel. Each of the two systems is composed of one electrical motor, motor controller and battery with battery management system. Two electrical motors are mounted on one shaft, forming a double-redundant engine unit.

The aircraft was developed with the motive of fully autonomous navigation. The control can be done either from the cockpit and/or from the ground station. In Elektra Two Solar UAS (Unmanned version), takeoff and landing by using a variety of sensors, fly back to the point of takeoff, GPS waypoint navigation and automatic path following while moving horizontally are a few recognizable characteristics of this aircraft. A large number of sensors are used in this optionally pilot system and for measuring various flight parameters in order to use in the system identification process. In particular MTi 100-series provide complete MEMS based IMU, VRU, AHRS and GNSS where it gives the linear acceleration and angular rate measurements along with the magnetometer measurements to estimate the orientation of the aircraft. GNSS gives the latitude, longitude and altitude measurements. Additionally, PSS-8 airdata probes located at the right wing gives measurements for true airspeed.

1.4 Applications

The applications of Elektra Two Solar UAS can be expanded to commercial, scientific and other applications, such as surveillance, policing, peacekeeping, and aerial photography. With the aid of a laser communication system or a radio system, data can be transmitted in real time over several 100 km. Elektra Two Solar has the capabilities to be used as a platform for creating 3D-mapping and can be used to take various types of measurements, such as air pollution at high altitude.

Such ultralight HALE aircraft are highly advantageous as they provide with numerous number of applications, including atmospheric observations, communication networks and earth observation objectives. HALE UAVs are getting recognized as they have the potential to substitute satellites due to high costs, necessity of rocket launch, and reliance of orbits intricate to the use of these spacecraft missions.

1.5 Outline of the thesis

The aircraft model is obtained using the measurements from the flight experiments for Elektra Two. This process of obtaining the mathematical models of the aircraft based on the measurements is called system identification. Chapter 2 provides the description about the identification method used which is called Two-Step method. It also provides a detailed description of the validation methods used for validating the model which is identified using the identification process. Chapter 3 deals with the detailed description of the chosen control strategy and the robustness analysis performed for the intended application. In Chapter 4, results and observations are presented for the identification process and also for the performance of the control design and the robustness analysis performed.

Chapter 2

Aircraft System Identification for Elektra 2

The system identification procedures build the mathematical models of the dynamic systems from the data recorded by various sensors of the aircraft. Some initial steps are performed in order to generate the experimental flight data with adequate information contents. The steps of the whole system identification process are presented in Fig. 2.1. The initial input design for the flight experiment is based on a priori model which is obtained from AVL solver.[6] The inputs are designed in order to excite some particular eigen modes. At first, the longitudinal model is targeted, the lateral model will also be identified later. Currently, only longitudinal modes are to be excited. (phugoid and short period). Also, an identifiability analysis was performed in order to choose the best input to identify the each derivative for the forces and moments of the aircraft model. Once the inputs are designed, the flight experiments are performed.

Once, the data has been recorded, it is extracted and processed in order to use in the identification process. It is significant to check and improve the quality of the recorded data as it can have a huge impact on the system identification process. There are various system identification techniques like output error method, filter error method and kalman filtering[7].

A method called Two step method has been applied to identify the aerodynamic model for Elektra Two. The Two step method is comprised of two stages namely flight path reconstruction in which the compatibility of the data is checked independent of the system parameter estimation [8], [9] and second, aerodynamic model identification in which force and moment parameters are estimated using linear regression [10]. This approach is capable of estimating measurement biases independently from the derivative terms, eliminating the need of correct initial guesses for the parameters like those in Output error method [11].

Various studies have presented the system identification procedures for different aircraft (Penguin BE and Elektra 1) using this approach of Two Step Method [8], [12], [13]. In some of

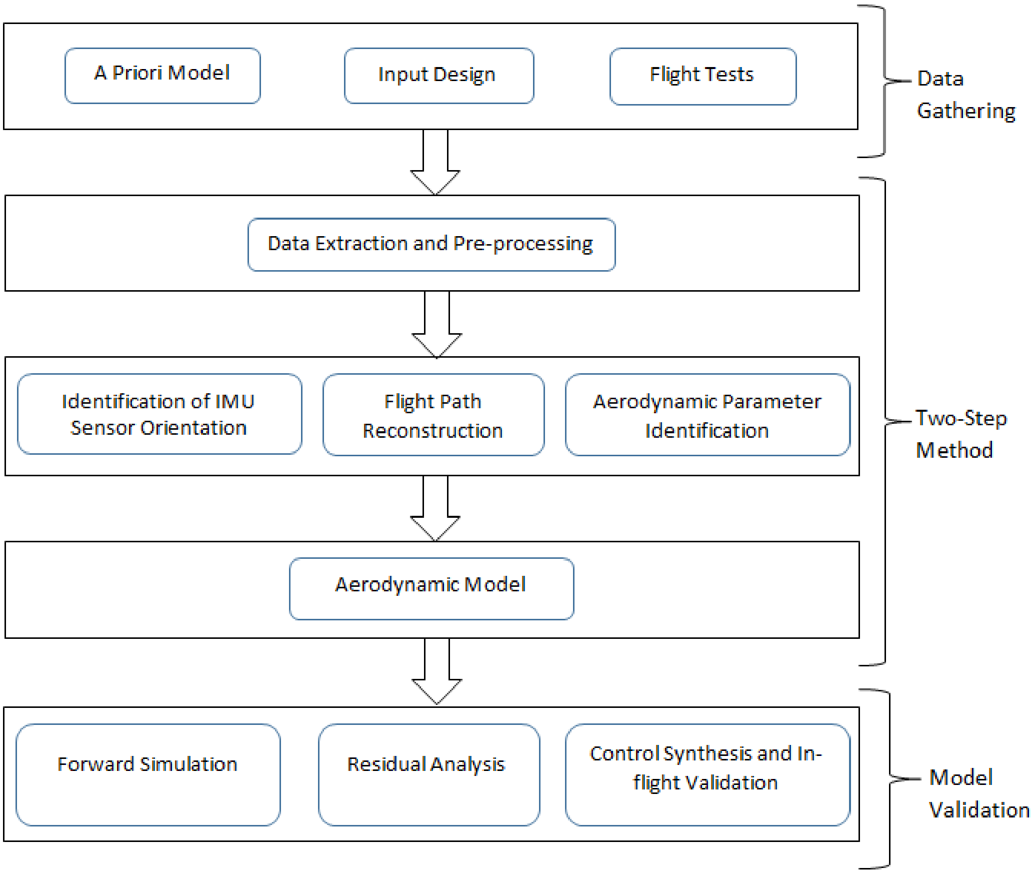
A Priori Model
Input Design
Flight Tests
Data Gathering
Data Extraction and Pre-processing
Identification of IMU Sensor Orientation
Flight Path Reconstruction
Aerodynamic Parameter Identification
Two-Step Method
Aerodynamic Model
Forward Simulation
Residual Analysis
Control Synthesis and In-flight Validation
Model Validation

Figure 2.1: Steps of System Identification Process

the studies, a stochastic approach based on an Extended Kalman Filter (EKF) has been applied in the first step, rather than the deterministic one [14], [15]. In this study, a method based on the maximum likelihood estimation approach is presented for the system identification of Elektra 2. It is observed that the deterministic approach provides better results when there is no accurate a priori knowledge about noise statistics which is the case in this study [16], [17].

Once a reliable aerodynamic model is obtained, it is further validated using various methods like performing a forward simulation to do a state level validation and performing a residual analysis. Finally, a controller synthesis is performed to complete the whole process. The further sections include the detailed description about the implementation of the Two-Step approach for identifying the model of the aircraft.

2.1 Data Extraction and Pre-Processing

Processing the experimental measured data before using it in the system identification process is a significant step in order to estimate an accurate aerodynamic model. In this pre-processing of the recorded data, the measured quantities are converted into correct units and transformed into required body frame of the aircraft. Hence, the definition of the body frame considered should be precisely defined. The origin is located at the centre of gravity of the aircraft, the x-direction is defined by the alignment of the vertical stabilizer pointing forward, the y-axis is defined using the x-axis and it lies in the horizontal plane of the aircraft. It is positive to the right and the z-axis is defined using the right hand rule, orthogonal to the other two axis, which comes out to be positive downwards.

In the given flight experiment, total 7 identification maneuvers exciting the phugoid maneuver were chosen for the system identification process out of more than 30 maneuvers performed. The flight data is separated into 2 sets: one which is used for the identification process, called identification set (containing maneuvers 1,3, 5 and 7) and the other which is only used to validate the already identified aircraft model,called validation set (containing maneuvers 2,4 and 6). Three main steps described in the next section were performed to extract the recorded data and to make it suitable to use in the identification process.

2.1.1 Importing the data

The first task done in the pre-processing of the flight data is to import the recorded flight data from the original folder, separate the desired signals in the time segments in which each maneuver was performed.

2.1.2 Processing of data

In certain cases, there are logging issues while recording the flight data in an experiment. Duplicate values are logged for the same time instant. In this task, all the duplicates present in the raw data must be removed. Another issue comes with the measurement of data with different sensors. In Elektra Two, each sensor has a different sampling rate (20, 33 and 50 Hz). Hence, the next step is to interpolate all signals to be in the same sampling frequency (50 Hz) and same time reference (the time vector is now the same for all the signals). Then, data from different sensors, which is measured in NED frame is converted to the aircraft body frame using the following transformation matrix.

$$T_B = \begin{bmatrix} \cos\theta\cos\psi & \cos\theta\sin\psi & -\sin\theta \\ -\cos\phi\sin\psi + \sin\phi\sin\theta\cos\psi & \cos\phi\cos\psi + \sin\phi\sin\theta\sin\psi & \sin\phi\cos\theta \\ \sin\phi\sin\psi + \cos\phi\sin\theta\cos\psi & -\sin\phi\cos\psi + \cos\phi\sin\theta\sin\psi & \cos\phi\cos\theta \end{bmatrix} \tag{2.1}$$

The motion variables in the kinematic equations (Eq.(2.3), Eq.(2.4), Eq.(2.5) and Eq.(2.6)) are measured with respect to center of gravity. Usually, the IMU sensors are not mounted exactly at the CG point of the aircraft, hence it needs to be corrected because if the accelerometer data is not in the required body frame, it is not possible to obtain an accurate model. Hence the accelerometer data needs to be transformed to CG in order to use these variables in the kinematic model. But these errors are rather small and the effect is so small that this transformation is omitted in this case. This transformation does not affect the results in the present case, hence this transformation is omitted.

The angular accelerations are obtained by doing numerical differentiation of the measured angular rates by using a smoothed differentiation filter [18]. Also, the accelerometer data is filtered using a zero-phase filtering to make the data less noisy for the system identification [18]. Although, all the signals are already sampled at a common sampling rate but it is important that the sampling frequency of the processed data and the identification process should match. Hence, all the measurements are resampled to the sampling rate used in the identification i.e. 20 Hz.

Also, the wind vector was computed using the information of true airspeed and ground speed measurements. As a first step, real airspeed is computed in aerodynamic frame and then transformed to body frame.Then, this airspeed was transformed to NED frame. The wind speed can be computed using the vector addition of this airspeed and the ground speed. However, the presented approach of Two Step approach Method is valid only in the case of constant wind, the wind computations were not used in the later steps of the system identification process. Although this yields an important information and can be used in other system identification approaches, as it will make the identification more realistic. As the state estimation will become more precise using this extra component of the wind affecting the states, a better model of the aircraft can be obtained.

2.1.3 Corrections

There can be several outliers like the range of the angles measured (were measured between 0 and 2π) can be different than to be used in the identification process (are to be used between 0 and π) in the recorded flight data. In this last step of processing the flight data, these type of outliers present in the data are removed and the flight data for each maneuver is segregated. The selected maneuvers for the identification set and the validation set are joined in a sequential order. Finally, they are saved in the separated files for identification and validation set.

2.2 Two Step Method

There are many system identification procedures which directly provide the final model of the aircraft but finding both the corrections in the states and the parameters of a system simultaneously is an arduous task. For an aircraft, there is a method called Two Step method which makes this task easier [19]. The first step of the Two Step approach is called flight path reconstruction or data compatibility check. The main objective of a data compatibility check is to ensure that the recorded measurements used for subsequent aerodynamic model identification are persistent and accurate. In order to increase the accuracy of the flight data and hence the aerodynamic model, an additional step is being performed before this first step of data compatibility check in order to adjust the orientations of the IMU sensors. This step is referred as identification of orientation of IMU sensor in the present thesis. The flight path reconstruction is also significant part of the Two-Step approach using the least squares technique to estimate aerodynamic derivatives [9], which is hence the second step of this approach. In the second step, with all the recorded measurement data, the aerodynamic forces and moments are reconstructed and the aerodynamic model of the aircraft is obtained. In order to obtain the aerodynamic model, the flight dynamics equations of aircraft motion to include systematic errors are adapted, sensor models are postulated, the techniques of parameter estimation are addressed.

2.2.1 Flight Dynamic Model

The 6DOF model for identifying the correct orientation of the accelerometer sensors and the data compatibility check is derived from the equations of motion of an aircraft [9]. In order to simplify, the aircraft is assumed to be a rigid body and the earth is assumed to be flat and stationary.

The nonlinear aircraft force equations of motion (translational and rotational motion) are shown in Eq.(2.2),

$$\begin{aligned} m(\dot{u} + qw - rv) + mg\sin\theta &= F_X \\ m(\dot{v} + ru - pw) + mg\cos\theta\sin\phi &= F_Y \\ m(\dot{w} + pv - qu) + mg\cos\theta\cos\phi &= F_Z \end{aligned} \tag{2.2}$$

where F_X, F_Y, F_Z correspond to the external (aerodynamic and thrust) forces. In order to use for the parameter estimation, the above equations are rewritten in state variable form.

$$\begin{aligned}
\dot{u} &= -qw + rv - g\sin\theta + a_x \\
\dot{v} &= -ru + pw + g\cos\theta\sin\phi + a_y \\
\dot{w} &= -pv + qu + g\cos\theta\cos\phi + a_z
\end{aligned} \tag{2.3}$$

where the a_x, a_y, a_z corresponds to F_X/m, F_Y/m, F_Z/m respectively and represent the accelerations along the three axes. Also, the angles θ and ϕ denote pitch and roll angles, respectively. The kinematic equations relating the Euler angles to the body-fixed rotational rates p, q, r are:

$$\begin{aligned}
\dot{\phi} &= p + q\sin\phi\tan\theta + r\cos\phi\tan\theta \\
\dot{\theta} &= q\cos\phi - r\sin\phi \\
\dot{\psi} &= q\sin\phi\sec\theta + r\cos\phi\sec\theta
\end{aligned} \tag{2.4}$$

The navigation equations are:

$$\begin{aligned}
\dot{x}_g &= u\cos\psi\cos\theta + v(\cos\psi\sin\theta\sin\phi - \sin\psi\cos\phi) + w(\cos\psi\sin\theta\cos\phi + \sin\psi\sin\phi) \\
\dot{y}_g &= u\sin\psi\cos\theta + v(\sin\psi\sin\theta\sin\phi - \cos\psi\cos\phi) + w(sin\psi\sin\theta\cos\phi + \cos\psi\sin\phi) \\
\dot{h} &= u\sin\theta - v\cos\theta\sin\phi - w\cos\theta\cos\phi
\end{aligned} \tag{2.5}$$

The corresponding moment equations completing the set of 6 DOF equations for an aircraft are given as:

$$\begin{aligned}
\dot{p} &= c_1 qr + c_2 pq + c_3 L + c_4 N \\
\dot{q} &= c_5 pr - c_6\left(p^2 - r^2\right) + c_7 M \\
\dot{r} &= c_8 pq - c_2 qr + c_4 L + c_9 N
\end{aligned} \tag{2.6}$$

where c_1 to c_9 are the terms containing the moments of inertia and are given below

$$\begin{bmatrix} c_1 \\ c_2 \\ c_3 \\ c_4 \\ c_8 \\ c_9 \end{bmatrix} = \frac{1}{\left(I_{xx}I_{zz} - {I_{xz}}^2\right)} \begin{bmatrix} I_{zz}\left(I_{yy} - I_{zz}\right) - {I_{xz}}^2 \\ I_{xz}\left(I_{zz} + I_{xx} - I_{yy}\right) \\ I_{zz} \\ I_{yz} \\ I_{xx}\left(I_{xx} - I_{yy}\right) + {I_{xz}}^2 \\ I_{xx} \end{bmatrix} \tag{2.7}$$

$$
\begin{aligned}
c_5 &= (I_{zz} - I_{xx})/I_{yy} \\
c_6 &= I_{xz}/I_{yy} \\
c_7 &= 1/I_{yy}
\end{aligned}
\tag{2.8}
$$

Eq.(2.3), Eq.(2.4), Eq.(2.5) and Eq.(2.6) represent the complete set of kinematic and dynamic relationships used for the identification of orientation of IMU sensors and the flight path reconstruction. Assuming all the necessary measurements are available the states can be estimated. Once the aircraft states are known, other variables like angle of attack α_k, angle of sideslip β_k true airspeed V_k and dynamic pressure q_{bar} can be computed.

$$
\begin{aligned}
V_k &= \sqrt{u^2 + v^2 + w^2} \\
\alpha_k &= \tan^{-1}(w/u) \\
\beta_k &= \sin^{-1}(v/V) \\
\bar{q} &= 1/2\rho V^2
\end{aligned}
\tag{2.9}
$$

Also, the sensor errors are estimated appending a model in terms of scale factor, bias and time delay to the recorded variables with purpose of reducing the errors.The sensor model is expressed as:

$$
y_m(t) = K_y y(t - \tau) + \Delta y \tag{2.10}
$$

It is noticed that the state equations for geodetic positions x_g and y_g are decoupled and they don't appear in the other set of equations. So they can be omitted without affecting the flight path reconstruction results. The moment equations are not used in the first step of the identification process, hence they can also be omitted. It can be noticed that $\dot{\psi}$ equation is also not coupled in other equations, so it could also be neglected, but as it aids the estimation of bias in the yaw rate r so it is retained. Hence, the state vector reduces to $[u\ v\ w\ \phi\ \theta\ \psi\ h]^T$

2.2.2 Identification of Orientation of IMU Sensor

The significance of this initial step is to make sure that the data obtained from the IMU sensor is in the required body-fixed coordinates. The motion variables in the kinematic equations are with respect to the body fixed coordinate system. There could be certain cases when the sensors are mounted at off-CG locations and hence the recorded data needs to be transformed to CG in order to use these variables in the kinematic model. However, the effect has been analyzed and was found to be negligible. Hence, this transformation is avoided in this case. In addition to correcting the data for this off-CG transformation, there is another type of correction that needs to be corrected which is caused due to sensor misalignment. If the alignment of the sensors is not properly oriented along the body-fixed coordinates, it can lead to cross coupling between the axes. An orientation error in the accelerometer data can cause acceleration along the sensor axis of sensitivity and along the other orthogonal axes also to be recorded. Hence, the recorded data is corrected for this misalignment. The correct accelerations along the body fixed coordinates is given by

$$\begin{bmatrix} a_x^B \\ a_y^B \\ a_z^B \end{bmatrix} = T_B \begin{bmatrix} a_{xm} \\ a_{ym} \\ a_{zm} \end{bmatrix} \tag{2.11}$$

where T_B is the transformation matrix which gives the transformation from the sensor frame to the aircraft body axes frame.

$$T_B = \begin{bmatrix} \cos\theta'\cos\psi' & \cos\theta'\sin\psi' & -\sin\theta' \\ -\cos\phi'\sin\psi' + \sin\phi'\sin\theta'\cos\psi' & \cos\phi'\cos\psi' + \sin\phi'\sin\theta'\sin\psi' & \sin\phi'\cos\theta' \\ \sin\phi'\sin\psi' + \cos\phi'\sin\theta'\cos\psi' & -\sin\phi'\cos\psi' + \cos\phi'\sin\theta'\sin\psi' & \cos\phi'\cos\theta' \end{bmatrix} \tag{2.12}$$

The rotation angles ψ’, θ’ and ϕ’ represent the orientation of the IMU sensor with respect to the body frame which is to be estimated in this initial step. These rotation angles are estimated by the Output Error Method comparing the integrated nonlinear state equations provided the measurements of linear accelerations and rotational rates are available from the recorded flight data. In the computation of correct orientation of the IMU sensor, both lateral and longitudinal measurements are used. The set of nonlinear equations used for the identification of the orientation of IMU sensor are shown in Eq.(2.13).

$$\begin{aligned} \dot{u} &= -qw + rv - g\sin\theta + a_x^B & u(t_0) &= u_0 \\ \dot{v} &= -ru + pw + g\cos\theta\sin\phi + a_y^B & v(t_0) &= v_0 \\ \dot{w} &= -pv + qu + g\cos\theta\cos\phi + a_z^B & w(t_0) &= w_0 \\ \dot{\phi} &= p + q\sin\phi\tan\theta + r\cos\phi\tan\theta & \phi(t_0) &= \phi_0 \\ \dot{\theta} &= q\cos\phi - r\sin\phi & \theta(t_0) &= \theta_0 \\ \dot{\psi} &= q\sin\phi\sec\theta + r\cos\phi\sec\theta & \psi(t_0) &= \psi_0 \\ \dot{h} &= u\sin\theta - v\cos\theta\sin\phi - w\cos\theta\cos\phi & h(t_0) &= h_0 \end{aligned} \tag{2.13}$$

where a_x^B, a_y^B and a_z^B are the linear accelerations in the body fixed coordinate frame. These accelerations are dependent on the orientation of the IMU sensor with respect to the body axes coordinate frame (as shown in Eq.(2.11)). The rotation angles ϕ', θ' and ψ' are the parameters to be estimated in this initial step of the system identification process. The sensor noise is ignored with an assumption of high precision measurements of the accelerations and the rotation rates. Hence, the state estimation reduces to be a simple numerical integration. With this assumption the model for this orientation estimation becomes:

$$\begin{aligned} \dot{x}(t) &= f\left[x(t), u(t), \Theta\right], x(t_0) = x_0 \\ y(t) &= g\left[x(t), \Theta\right] \\ z(t_k) &= y(t_k) + v(t_k) \end{aligned} \tag{2.14}$$

where the state, input and observation vectors are given by

$$\begin{aligned} x &= [u\ v\ w\ \theta\ \phi\ \psi\ h]^T \\ u &= \left[a_x\ a_y\ a_z\ p\ q\ r\right]^T \\ y &= [V\ \alpha\ \beta\ \phi\ \theta\ \psi\ h]^T \end{aligned} \tag{2.15}$$

and the unknown parameters are given as:

$$\Theta = [\phi'\ \theta'\ \psi']^T \tag{2.16}$$

In order to estimate the vector of unknown instrument errors, the Output Error Method for nonlinear systems is applied on this state space model[20]. Also, the covariance matrix of the measurement noise is computed. This is done by adjusting the parameters to minimize the error between measured and estimated states. Levenberg-Marquadt method has been used to perform the minimization and the numerical integration was performed using a fourth order Runge-Kutta method [21]. The accelerations are then reoriented and transformed to body fixed coordinate frame in order to use in the next step of flight path reconstruction.

2.2.3 Flight Path Reconstruction

The significance of flight path reconstruction or data compatibility check is to demonstrate that the measured data is compatible and consistent to use for the identification of the aircraft model [22]. In order to identify a precise model, it is important that data is error free, which can be achieved by properly defining the systematic errors by evaluating the 6DOF rigid-body kinematic and dynamic equations using the recorded flight variables. As the least sqaure methods are very susceptible to systematic errors like scale factors, zero-shift biases and time lags and noises, the other deterministic approaches like Output Error or Filter Error methods are preferred as they also allow noise estimation. The aircraft stability and control derivatives can be computed by the Two Step Method, where in this work, the flight path reconstruction has been performed using Output Error Method.

In this first step of checking the data compatibility, both lateral and longitudinal measurements are used. But, only the estimated biases in the longitudinal model are used as inputs in the next step. The updated set of nonlinear state equations along with the sensor model which are used in the flight path reconstruction are shown in Eq.(2.17)

$$\begin{aligned}
\dot{u} &= -\left(q_m - \Delta q\right) w + \left(r_m - \Delta r\right) v - g \sin\theta + \left({a_x}^{CG} - \Delta a_x\right), && u\left(t_0\right) = u_0 \\
\dot{v} &= -\left(r_m - \Delta r\right) u + \left(p_m - \Delta p\right) v - g \cos\theta \sin\phi + \left(a_y^{CG} - \Delta a_y\right), && v\left(t_0\right) = v_0 \\
\dot{w} &= -\left(p_m - \Delta p\right) v + \left(q_m - \Delta q\right) u - g \cos\theta \cos\phi + \left(a_z^{CG} - \Delta a_z\right), && w\left(t_0\right) = w_0 \\
\dot{\phi} &= \left(p_m - \Delta p\right) + \left(q_m - \Delta q\right) \sin\phi \tan\theta + \left(r_m - \Delta r\right) \cos\phi \tan\theta, && \phi\left(t_0\right) = \phi_0 \\
\dot{\theta} &= \left(q_m - \Delta q\right) cos\phi + \left(r_m - \Delta r\right) \sin\phi, && \theta\left(t_0\right) = \theta_0 \\
\dot{\psi} &= \left(q_m - \Delta q\right) \sin\phi \sec\theta + \left(r_m - \Delta r\right) \cos\phi \sec\theta, && \psi\left(t_0\right) = \psi_0 \\
\dot{h} &= u \sin\theta - v \cos\theta \sin\phi - w \cos\theta \cos\phi, && h\left(t_0\right) = h_0
\end{aligned} \tag{2.17}$$

where Δa_x, Δa_y, Δa_z are the biases in the measured linear acceleration at the CG point and Δp, Δq, Δr are the biases in the rotational rate measurements. These are the biases to be estimated in the first step of the system identification process. Assuming that the accelerations and the rotation rates are measured with high precision, the sensor noise in the variables can be neglected such that the data compatibility check is deterministic which reduces the state estimation to be a simple numerical integration [9]. With this assumption the model for this instrument error estimation becomes:

$$\begin{aligned}
\dot{x}\left(t\right) &= f\left[x\left(t\right), u\left(t\right), \Theta\right], x\left(t_0\right) = x_0 \\
y\left(t\right) &= g\left[x\left(t\right), \Theta\right] \\
z\left(t_k\right) &= y\left(t_k\right) + v\left(t_k\right)
\end{aligned} \tag{2.18}$$

where the state, input and observation vectors are given by

$$\begin{aligned} x &= [u\ v\ w\ \theta\ \phi\ \psi\ h]^T \\ u &= \left[a_x\ a_y\ a_z\ p\ q\ r\right]^T \\ y &= [V\ \alpha\ \beta\ \phi\ \theta\ \psi\ h]^T \end{aligned} \tag{2.19}$$

and the unknown parameters are given as:

$$\Theta = \left[\Delta a_x\ \Delta a_y\ \Delta a_z\ \Delta p\ \Delta q\ \Delta r\right]^T \tag{2.20}$$

In order to estimate the vector of unknown instrument errors, the Output Error Method for nonlinear systems is applied on this state space model[20] similar to the the previous step of estimating the orientation of the IMU sensor. After estimating the biases, the longitudinal forces and moments acting on the aircraft could be reconstructed using the corrected linear accelerations and angular rates.

2.2.4 Aerodynamic Model Identification

The second step of Two Step Method is the identification of force and moment derivatives which is done using linear regression[23]. Once the linear acceleration and angular rate measurements have been reoriented and corrected, the reconstruction of the linear forces (aerodynamic and propulsion forces) and moments is feasible to obtain. In order to do this, the mathematical expressions for the longitudinal forces and moments are considered as linear combinations of inputs and states, as shown in Eq. (2.21)

$$\begin{aligned} X &= X_0 + X_u u + X_w w + X_q q + X_{\delta e}\delta e + X_{\delta t}\delta t \\ Z &= Z_0 + Z_u u + Z_w w + Z_q q + Z_{\delta e}\delta e \\ M &= M_0 + M_u u + M_w w + M_q q + M_{\delta e}\delta e \end{aligned} \tag{2.21}$$

In Eq.(2.21), the left hand side, X, Z and M correspond to reconstructed axial and normal forces, and the pitching moment, respectively. On the right hand side, the constant parameters are the force and moment coefficients that define the amount of force and moment that is generated by each variable and are called concise derivatives [24]. In short, the constant terms correspond to the first order terms of Taylor series expansion of the left hand side forces and moments with respect to each parameter on the right hand side. Moreover, the terms X_0, Z_0 and M_0 correspond to constant biases in the force and moment equations. The objective of this step is to achieve the best fit between the reconstructed forces and moments from the accelerations corrected from the previous step and the ones which are obtained by computing the linear polynomials from Eq. (2.21). From these force and moment parameters, a complete aerodynamic model is obtained.

2.3 Model Validation

Model validation is an integral part of the system identification procedure. In the process of model validation, it is checked if the simulated and the measured data correspond to each other. It is important to check the accuracy of the model that has been identified in the Two Step method. The identified model can be analyzed using various criteria. Several methods to validate the identified model can be broadly classified as: 1) standard deviations of the parameter estimates, 2) correlation coefficients among the estimates, 3) goodness of fit (i.e., value of the cost function being minimized), 4) model deficiencies in terms of residual control inputs (inverse simulation: is the process of calculating desired controls, for the given system model and response), 5) statistical analysis of residuals (bias, variance, covariance, and power spectral density), 6) plausibility of estimates(to check estimates from the plausibility of the estimates from physics of the dynamical system.), and 7) model predictive capability (by comparing the flight measured system responses with those predicted by the model)[9]. Some of these criteria like Goodness of Fit, Theil's Inequality Coefficient and validation using the forward simulation have been performed.

2.3.1 Metrics

In order to check the accuracy of the simulated data, two statistical measures were applied at the state level, Goodness of Fit (GOF) and Theil's Inequality Coefficient (TIC). The Normalized Mean Square error (NMSE) has been evaluated as a GOF metric, to estimate the overall deviations between measured and estimated parameters. The values of NMSE can range between $-\infty$ and 1 where negative values mean that a straight line matches the reference better than the estimated value, with $-\infty$ meaning the worst possible fit, whereas positive values indicate that the estimate fits better than a straight line. A perfect match between the data is indicated by a value one.

However, in comparison to GOF, Theil's Inequality Coefficient provides a better intuition about the correlation between the measured and estimated data. As the states are dynamic, the NMSE measurements can be inadequate for comparing the estimated data. The values of TIC range between 0 and 1. A lower values indicates a better fit. TIC values < 0.3 indicate a good fit with the data.

In addition to these measures, two more metrics were applied in order to validate the accuracy of the results obtained from the Two step method. R^2 and Normalized Root Mean Square Error (NRMSE) have been applied in order to check the force and moment estimations. R^2 is the proportion of variance in the dependent variable predictable from the independent variable. Its value varies between 0 and 1. Zero designates an estimate fitting worse than a straight line and 1 indicates a perfect match. The Normalized Root Mean Squared Error is the ratio of RMSE (Root mean squared error) and the variable range. The value of NRMSE range from 0 to 1, where smaller the values, better fit and 0 indicates the best fit. The characteristics of the validation metrics like range, best and worst values used for validating the model are presented in Table (2.1).

Table 2.1: Characteristics of Validation metrics

Metrics	Range	Best match	Worst match	Parameters
GOF (NMSE)	$-\infty \sim 1$	1	$-\infty$	states
TIC	$0 \sim 1$	0	1	states
R^2	$-\infty \sim 1$	1	$-\infty$	forces and moments
$NRMSE$	$0 \sim 1$	0	1	forces and moments

2.3.2 Forward Simulation for State-Level Validation

The final output of the system identification process is the aerodynamic longitudinal model which is in the form of linear expressions for the total longitudinal forces and moments acting on the aircraft. In order to avoid the extensive computations to linearize the nonlinear 6DOF equations of motion, they are instead used in the nonlinear form itself in the system identification process and hence, making the algorithm more practical.

The identified aerodynamic model is used to generate the longitudinal states using the longitudinal 6DOF dynamic equations as shown in Eq.(2.22). The longitudinal states are then compared to the ones that were recorded in the flight experiment. This type of validation is referred as forward simulation. The lateral states are used from the recorded measurements and the lateral angular rates are used from the measurements corrected with the estimated biases that were computed in the first step of the identification process.

$$\begin{aligned}
\dot{u} &= \frac{X}{m} - qw + (r_m - \Delta r)v_m - g\sin\theta \\
\dot{w} &= \frac{Z}{m} + qu + (p_m - \Delta p)v_m - g\cos\theta\cos\phi_m \\
\dot{q} &= \frac{1}{I_{yy}}\left(M + \left((r_m - \Delta r)^2 - (p_m - \Delta p)^2\right)I_{xz} + (p_m - \Delta p)(r_m - \Delta r)(I_{zz} - I_{xx})\right) \\
\dot{\theta} &= q\cos\phi_m - (r_m - \Delta r)\sin\phi_m
\end{aligned} \tag{2.22}$$

where m is the mass of the aircraft; Iyy, Izz, Ixx, and Ixz denote the aircraft moments of inertia and a product of inertia with respect to the axes indicated in the subscripts; X, Z, M are the longitudinal forces and moments estimated using the linear derivative model in the second step ; subscript m stands for measured lateral states, and Δ stands for the estimated biases in lateral angular rates.

2.3.3 Validation Set

As another measure to validate the aerodynamic model obtained from the system identification process, the estimated force and moment parameters are tested in the part of the flight data which was not used in the identification. This flight data is comprised of phugoid maneuvers that were not used in the identification and were save separately as validation set.

Just similar to the identification process, the identification of the orientation of the IMU sensor is performed and then the first step, data compatibility check is performed with the different set of maneuvers in the validation set and the respective biases in the linear accelerations and the angular rates are estimated for these maneuvers and the states are corrected. Then, for the second step, the previously estimated longitudinal force and moment parameters from the identification set are used directly to generate the aerodynamic model rather than identifying them again. Using this aerodynamic model, a forward simulation is performed to generate the longitudinal states in order to further validate the estimated aircraft model.

Chapter 3

Control Design

3.1 Initial Control Design

The initial PID based control design involved the tuning in flight using the Ziegler-Nichols method. The simplicity of the PID controller makes it the most versatile and most widely used control approach in almost all kind applications. A nominal PID Controller comprises of a feedback loop with a Proportional gain, Integral gain in order to eliminate the steady state error and the derivative term to predict how fast error is changing.

However, in many applications, only one or two terms are used to provide the appropriate control to the system. This can be achieved by forcing the unutilized terms to zero and then the controller is called PI, PD, P or I controller accordingly. Many of the applications like in tele-manupulation PD controllers are used. Also, PI controllers are used often in aviation, as the derivative action is sensitive to measurement noise, whereas the absence of an integral term may prevent the system from reaching its target value because of the steady state error. PID controllers only rely on the response of the measured process variable without depending on the knowledge of the model of the process [25].

PID controller is used for diverse applications from automation to even temperature and heat sensors. Keeping in mind the advantages of a PID controller and maintaining the simplicity, PID controller is maintained for this design. Although, many of the advanced control approaches are designed using the PID control as their base [26]. Hence, an optimization based tuning method is being used in this study to design the optimal gains for the PID controller.

3.2 Optimization based Controller Tuning

The various PID loop tuning methods involve heuristic tuning of PID parameters based on the dynamic model parameters, Ziegler-Nichols method and other optimization based tools. For most modern applications, the use of manual calculation methods is reduced as it is neither robust nor optimal. The controller gains can also be determined using a low order approximation. Although, such methods lead to suboptimal solutions. Instead, PID tuning and loop optimization software are used to ensure consistent results. These software tools gather the data, develop process models, and suggest optimal tuning approach. Many software tools can even develop tuning by gathering data from reference changes.

Hence, a similar approach to optimize the controller gains is used in the present design to make the control design process more efficient. A nonlinear optimization algorithm is used which calculates the minimum of a multivariable function without calculating the gradient. The optimization is based on the Nelder-Mead simplex algorithm. [27]. The objective function is being minimized without involving differentiation by only using the function value, in this algorithm. This optimization technique is used to tune the core gains of TECS (Total Energy Control System) and in the inner and outer loops of the longitudinal autopilot. For this tuning method, it is only obligatory to provide an initial value as well as the upper and lower bounds of the different variables of the system to the optimization algorithm.

The control parameters (K_T and K_{iT}) must be selected to optimize the step response (say, for airspeed) for a system. There can be various measures to evaluate the system's step response for different variables. Some of these measures considered for this study are defined as below.

- **Rise time** (t_r): Time required for the response to go from 10 to 90% of its final value.
- **Maximum overshoot** (OS_{max}): Difference between maximum and final value in underdamped systems.
- **Maximum derivative of control signal** ($|\dot{u}|$): Maximum rate of change of control command.
- **Integral Squared Error** (ISE): Integral of squared error from time zero to infinity.
- **Integral Absolute Error** (IAE): Integral of absolute value of error from zero to infinity.
- **Integral Time-weighted Absolute Error** (ITAE): Integral of absolute value of error multiplied by the time, from zero to infinity

Many combinations of these performance measures were tested in order to find an appropriate objective function for the required application. The objective function f is assumed to be a function of these measures and is given in Eq.(3.1)

$$f\left(t_s, OS_{\max}, |\dot{u}|, ISE, ISA, ISCD\right) = F\left(K_T, K_{iT}\right) \tag{3.1}$$

The main objective is to find the optimal values of the gains, such that

$$f_{opt} = \underset{(K_T>0, K_{iT}>0)}{min} F\left(K_T, K_{iT}\right) \tag{3.2}$$

In the given problem, f is considered as a linear combination of these performance measures. As each of these performance measures depend on K_T and K_{iT}, hence also the objective function. A final combination of these performance measures was considered after testing many different combinations. The task of selecting the weights in can vary according to the design objectives and applications.

3.3 Stability of the Control System

In order to evaluate the effectiveness of the optimization method for gain tuning, the stability margins of the longitudinal dynamics are compared before and after the optimization. Frequency response approach involves simple tests like checking the stability margins in the bode plots [28], Nyquist and Nichols plots. For time domain analysis, the step response is one of the basic measures to analyse the performance of the system.

The analysis involved checking the stability margins from a bode plot for analysing the behaviour of the system. Bode plot is a combination of a Bode magnitude plot that presents the magnitude (usually in decibels) of the frequency response and a Bode phase plot presenting the phase shift. The measures expressing the stability involve mainly gain and phase margins in the bode plot. Following measures of the stability of systems are normally used in frequency domain:

- **Phase crossover frequency** :The phase crossover frequency is the frequency at which the phase angle first reaches -180°.
- **Gain margin** : This is the factor by which the gain must be multiplied at the phase crossover to have the value 1. A stable control system should have a positive gain margin.
- **Gain crossover** : This is the frequency at which the open-loop gain first reaches 1.

- **Phase margin** : This provides the number of degrees by which the phase angle is smaller than -180° at the gain crossover [29]. A stable control system has a positive phase margin.

Out of these measures, the gain and phase margins are used to compare the behaviour for the system with the initial control design and the optimization based control design considering the transfer function between the airspeed and the desired airspeed.

Apart from this, the two systems are also compared using the step response for airspeed by relating various characteristics of the step response to its time behavior. These characteristics are overshoot, rise time and settling time which are used to validate the capabilities of the optimization based control design (as shown in Fig. 3.1). The overshoot considered is the percentage overshoot relative to the set-point value for each state. The settling time is the time it takes for the error between the response and the set-point to the fall to within 2% of the set-point. Peak is the maximum absolute value of the response and the time at which peak occurs is called the peak time. Rise time is the time it takes for the response to rise from 10% to 90% of the steady-state response [2]. Settling time and overshoot are considered as the measures to analyse the control design for the present study.

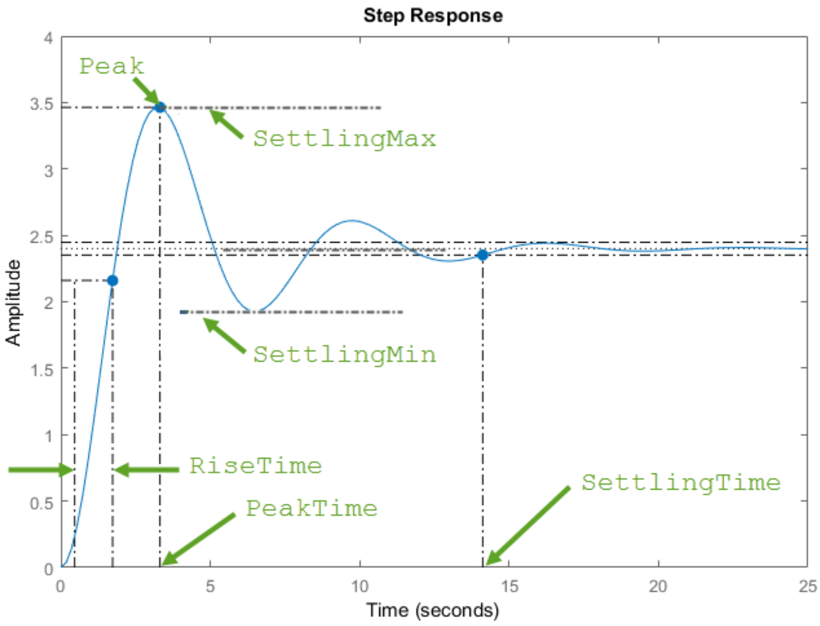

Figure 3.1: Stability margins in a Step Response [2]

3.4 Robustness Analysis

It is important to check if the controller designed is robust when it encounters some sudden changes in the external environment or the internal system model parameters. Robustness analysis provides an approach to observe the behaviour of the system model and the control design of problem situations when uncertainties are present. Uncertainties can enter the process of aircraft design in many places, it can be at the modelling level, control design level or even due to the external disturbances like sudden gust disturbance.

An estimate of the influence of the mentioned uncertainties can be made by a systematic variation of design parameters that mainly affect the aircraft model, the engine and aerodynamic properties, in order to validate the software tool developed. The uncertainties can be formulated by a set of random variables that transfer a deterministic reference model of an aircraft model and control design to a probabilistic model [30]. Probabilistic model interpretation are often obtained by sampling techniques like the basic Monte Carlo (MC) method to comprehend about the robustness of the reference aircraft model. However, many of these simulations are required for accurate statistics. Monte Carlo Simulations are widely used for sensitivity and robustness analysis. A similar approach has been used in the present study to analyse the robustness of the control system.

3.4.1 Effect of Wind Gust

In order to evaluate the effectiveness of the controller, its behaviour is tested for the effect of gust disturbance. The main objective is to test if the controller tuned with the optimization based tuning method is optimal even with these kind of disturbances. Monte Carlo simulations are performed to provide the system with a random input of a gust disturbance to understand the impact of turbulence in the external environment. The system must return to its normal steady condition after the disturbance settled down [31].

A gaussian crosswind and tailwind with mean of 5 m/s and standard deviation of 0.06 is considered to analyse the present system. Fig. 4.16 and Fig. 4.17 show the distribution of gust disturbance generated using the Monte Carlo experiments. The outputs can be chosen according to the simulation set and the application in a Monte Carlo simulation. In the present study, the outputs considered involve maximum overshoot and undershoot, ITAE criteria and the mean absolute error and the settling time after the gust disturbance.

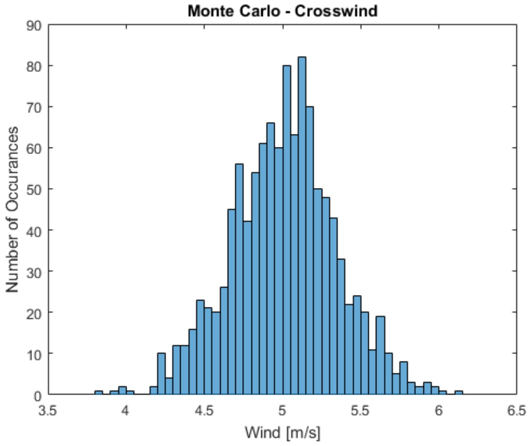

Figure 3.2: Distribution of Crosswind

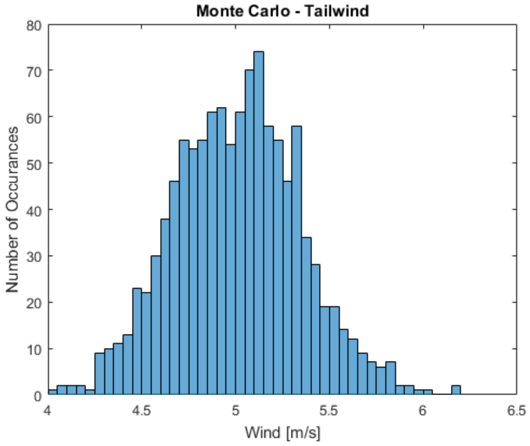

Figure 3.3: Distribution of Tailwind

3.4.2 Monte Carlo Simulations for Parametric Variations

The uncertainties in the estimated force and moment parameters in the system identification process are considered in this section. In this case, Monte Carlo method is used in order to formulate the set of random variations in the estimated force and moment parameters to test the robustness of the optimization based control design. Hence, the behaviour of the system model and the control design is analysed for a random set of force and moment parameters in a given range generated using Monte Carlo simulations.

In this case, along with the external gust disturbance, the identified longitudinal force and moment model parameters (from the system identification process) are also disturbed randomly in a defined range of 5% using Monte Carlo simulations. The disturbance in the model parameters is designed as a normal distribution with mean at their identified values using the system identification process and a standard deviation of 0.01. It can be noted that the Monte Carlo experiments presented in this thesis were performed with more than 1000 evaluations each, which is an adequate number to prove the robustness of the design.

Chapter 4

Results and Observations

4.1 System Identification

The results of the two step system identification process are presented in this section. The predicted orientation of the IMU sensor in the initial step is presented. The biases resulting from the flight path reconstruction and the aerodynamic model identification are presented in this section.

4.1.1 Identification of Orientation of IMU sensor

The results of this initial step of identifying the orientation of the IMU sensor with respect to body-fixed coordinate system are presented in a batch of four different phugoid maneuvers which are separated by black vertical lines. A comparison of measured longitudinal states of the aircraft is done with the estimated states after identifying the orientation of IMU sensor.

The values of rotation angles (in degrees) about different body axes which were identified in this initial step of system identification approach are presented in Table 4.1. It can be noticed that the orientation does not seem to be consistent for each different maneuver especially for heading angle, this is because of the problems encountered in the heading measurements. During the flight experiment, it was observed that the heading measurements were drifting because of the problems in the sensor. This is also clearly visible from the identified orientation. Except heading angle, the orientations about other axes are more consistent, hence the accelerations were reoriented and the states were corrected with these estimates. A comparison of the measured states and the estimated states after re-orientating the accelerometer data has been presented in Fig. (4.1). The reason for the drift in the lateral velocity possibly is the drift in the heading measurements. These states are used in the further step of flight path reconstruction for estimating biases and aerodynamic model identification.

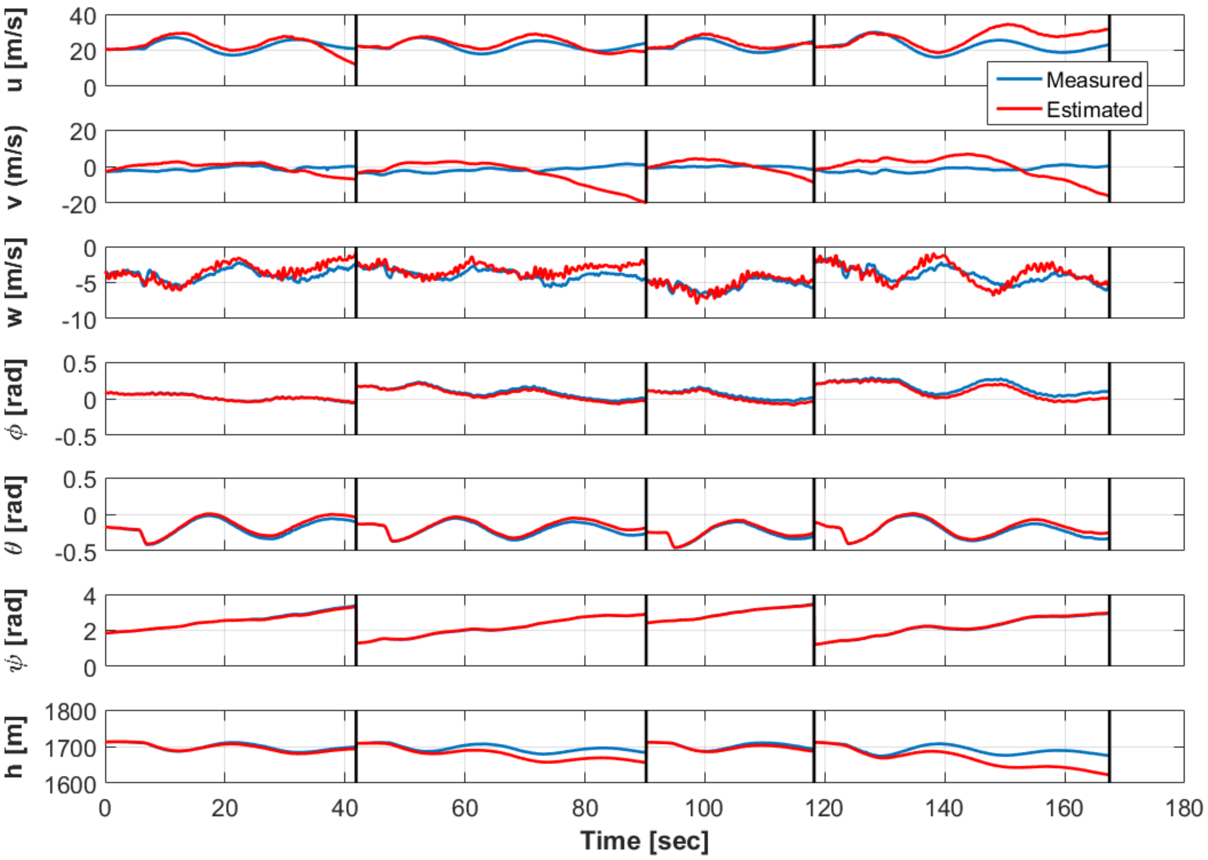

Figure 4.1: Measured longitudinal and lateral states and states generated from the integration of the 6DOF equations of motion with corrected accelerations: Identification Set

Table 4.1: Orientation of IMU sensor w.r.t. body axes

Orientation	Maneuver 1	Maneuver 2	Maneuver 3	Maneuver 4
ϕ’	-11.6	-3.28	-10.41	-6.41
θ’	-7.01	-2.75	-9.16	-9.02
ψ’	-10.44	27.13	-1.75	-26.81

4.1.2 Flight Path Reconstruction Results

In flight path reconstruction, the biases in linear accelerations and angular rates have been estimated. The comparison of the estimated states using the Two step method and the measured states which have been reoriented using the results identified in the previous step are compared as shown in Fig. 4.2. The longitudinal states are providing a good match when compared with the recorded data. However, the match between lateral velocity v and the recorded lateral velocity is not so good, but as explained earlier the drifting heading measurements cause aircraft lateral instability which is possibly the cause for the poor match for lateral velocity.

The values of the biases are calculated separately for each maneuver performed in the identification process because many times the biases of same nature can present different dimensions and different signs. It can be seen from Table 4.7 that the biases for linear accelerations (in m/s) and angular rates (in radians) are a little different for each maneuver yet quite close to each other. Hence, the overall estimate is considered to be a good match. The states are then corrected with these estimated biases and then used for the second step of aerodynamic model identification.

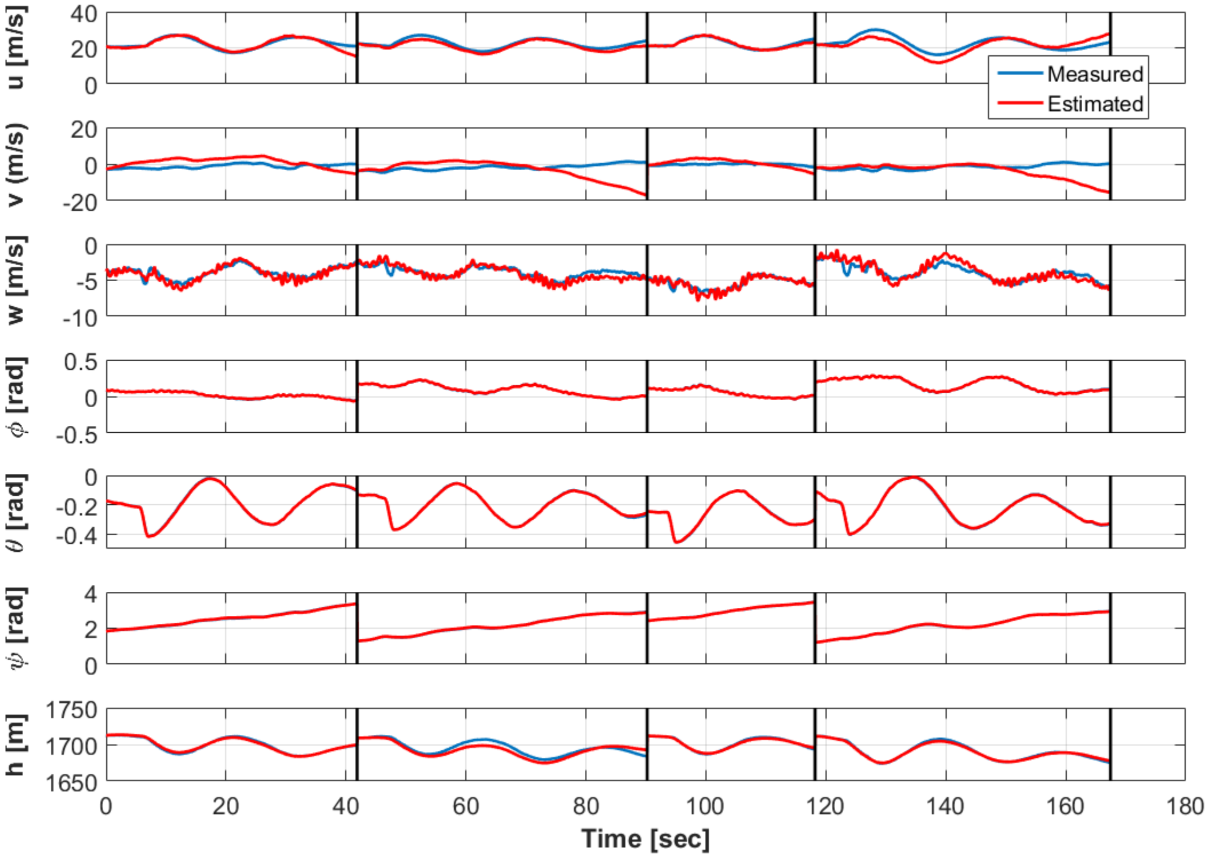

Figure 4.2: Measured longitudinal and lateral states and states generated from the integration of the 6DOF equations of motion with estimated biases added: Identification Set

4.1.3 Aerodynamic Model Identification

As the biases for the linear accelerations and angular rates have been already identified in the flight path reconstruction, the actual forces and moments acting on the aircraft during the flight can be estimated. In order to find the force and moment derivatives, a linear regression has been

Table 4.2: Estimated measurement biases for each maneuver

Orientation	Maneuver 1	Maneuver 2	Maneuver 3	Maneuver 4
b_{ax}	0.293	0.274	0.225	0.250
b_{ay}	-0.014	0.248	0.211	0.666
b_{az}	-0.051	-0.0402	-0.0392	-0.0945
b_p	-0.001	-0.0016	-0.0028	-0.0025
b_q	-0.0014	7.19×10^{-04}	5.8×10^{-04}	9.6×10^{-05}
b_r	-0.0011	3.3×10^{-04}	-5.5×10^{-04}	8.5×10^{-04}

performed.

Ordinary linear square method was used to estimate the longitudinal force and moment derivatives. Later, constrained linear square method was used to further improve the values of these force and moment derivatives in order to make the derivatives in correct range of magnitude and also to adjust the signs of each derivative. The derivatives obtained should be checked for signs and magnitudes and the ones which are were not relevant, were corrected by constraining their range using constrained linear square method. A comparison of estimated longitudinal forces and moments computed using constrained and unconstrained linear square method has been presented with the longitudinal forces and moments reconstructed using the the direct substitution of raw measurements into the aircraft dynamics equations in Fig.4.3.

It can be observed from Fig. 4.3 that the longitudinal forces and moment derivatives generated using the constrained linear square method provide a better fit than the ones obtained using the unconstrained linear square method. The final set of force and moment derivatives which were identified using constrained linear square method are presented in Table 4.3. It is observed that the signs and the range of the magnitudes are being taken care of according to the definitions of each derivative. It can be observed (from Table 4.3 that the throttle derivative, $X_{\delta t}$ is huge, which is not accurate. But the experiment was performed at a constant throttle which makes it difficult to identify the throttle component accurately. In future, the flight test data can be provided with a variable throttle, which can make it easier to identify the throttle derivative. Moreover, a nonlinear engine model can be used instead of identifying these components together with the aerodynamic forces and moments.

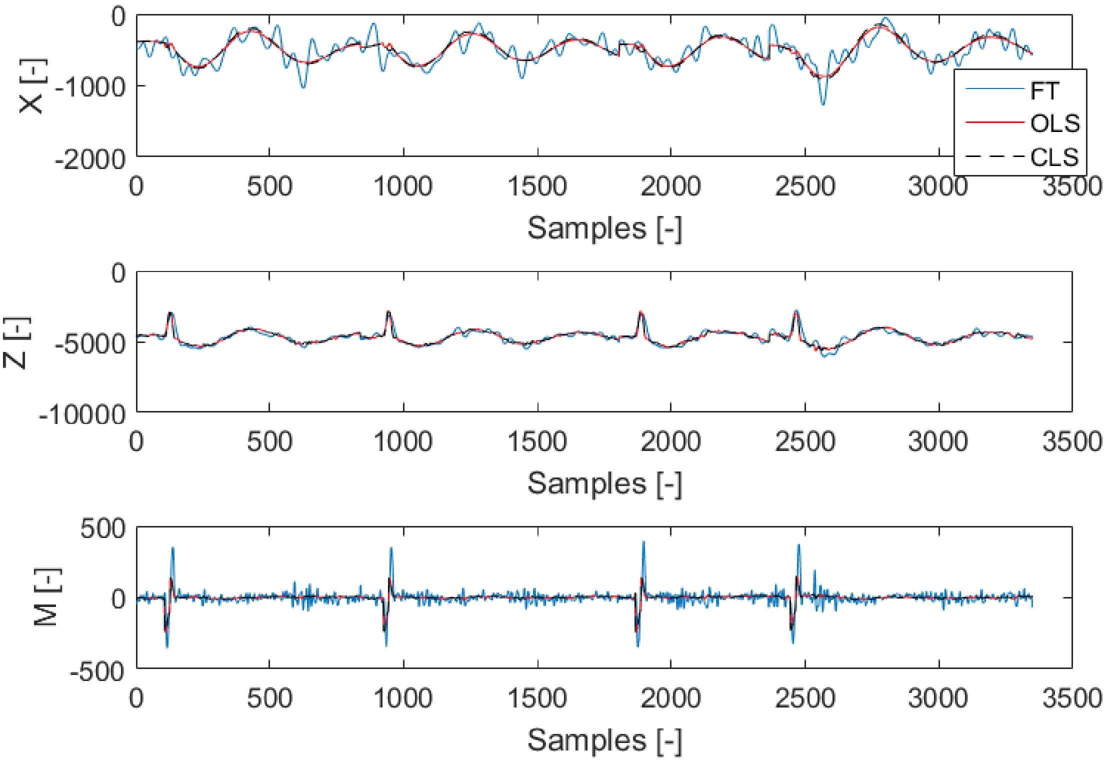

Figure 4.3: Reconstructed forces and moments, and forces and moments from linear regression: Identification set

Table 4.3: Values of longitudinal force and moment derivatives using linear regression

Axial Force	Value	Normal Force	Value	Pitching Moment	Value
X_0	-7030.2	Z_0	-3892.3	M_0	-236.91
X_u	-48.16	Z_u	-34.84	M_u	6.995
X_w	5.74	Z_w	-0.0014	M_w	-2.017
X_q	-114.7	Z_q	-8070.2	M_q	-654.74
$X_{\delta e}$	-448.5	$Z_{\delta e}$	-0.0179	$M_{\delta e}$	-2685
$X_{\delta t}$	12323.8				

4.2 Validation

4.2.1 Statistical Metrics

Various statistical measures were applied at the state level in order to check the accuracy of the simulated data from the identification process of the aircraft model. Table 4.4 depicts the Goodness of Fit (GOF) values and Theil's Inequality Coefficient (TIC) values for the estimated states in the first step, flight path reconstruction of the system identification process. It can be seen from the GOF and TIC values that all the longitudinal states have achieved a good match, whereas the lateral velocity doesn't depict a good match which could be due to the problems in the heading sensor as mentioned earlier.

Table 4.4: Statistical measures of the reconstructed states using flight path reconstruction: Identification Set

Measure	u	v	w	ϕ	θ	ψ	h
GOF	0.567	-13.2	0.703	0.999	0.999	0.999	0.93
TIC	0.043	0.746	0.063	0.008	0.004	0.002	0.0008

Table 4.5 represents the statistical measures of the estimated longitudinal force and moments using the constrained linear square method. It can be observed that R^2 values depicts a really good match. The values of NRMSE values are small as expected for a good fit.

Table 4.5: Statistical measures of the longitudinal force and moments using Two step method: Identification Set

Measure	X	Z	M
R^2	1	0.99845	1
NRMSE	$9.95 \times 10^{-}3$	0.0061	0.000137

4.2.2 Validation Set

The validation set refers to a different set of flight data which was not used in the identification process. It comprised of three phugoid maneuvers. The procedure of system identification was repeated for this validation set to check the credibility of the estimated aerodynamic model.

The states reoriented after identifying the orientation of the IMU sensors are compared to the one which were recorded in the flight experiment as shown in Fig. (4.4). It is observed that the states provide a good match except the lateral velocity, v, similar to the identification set. The values of orientation of the IMU sensor with respect to body axes corresponding to each maneuver of the flight data is expressed in Table 4.6. The values for the heading are not very consistent due to the problems with the heading sensor of Elektra Two which is the basic cause of not a good match here for the validation data.

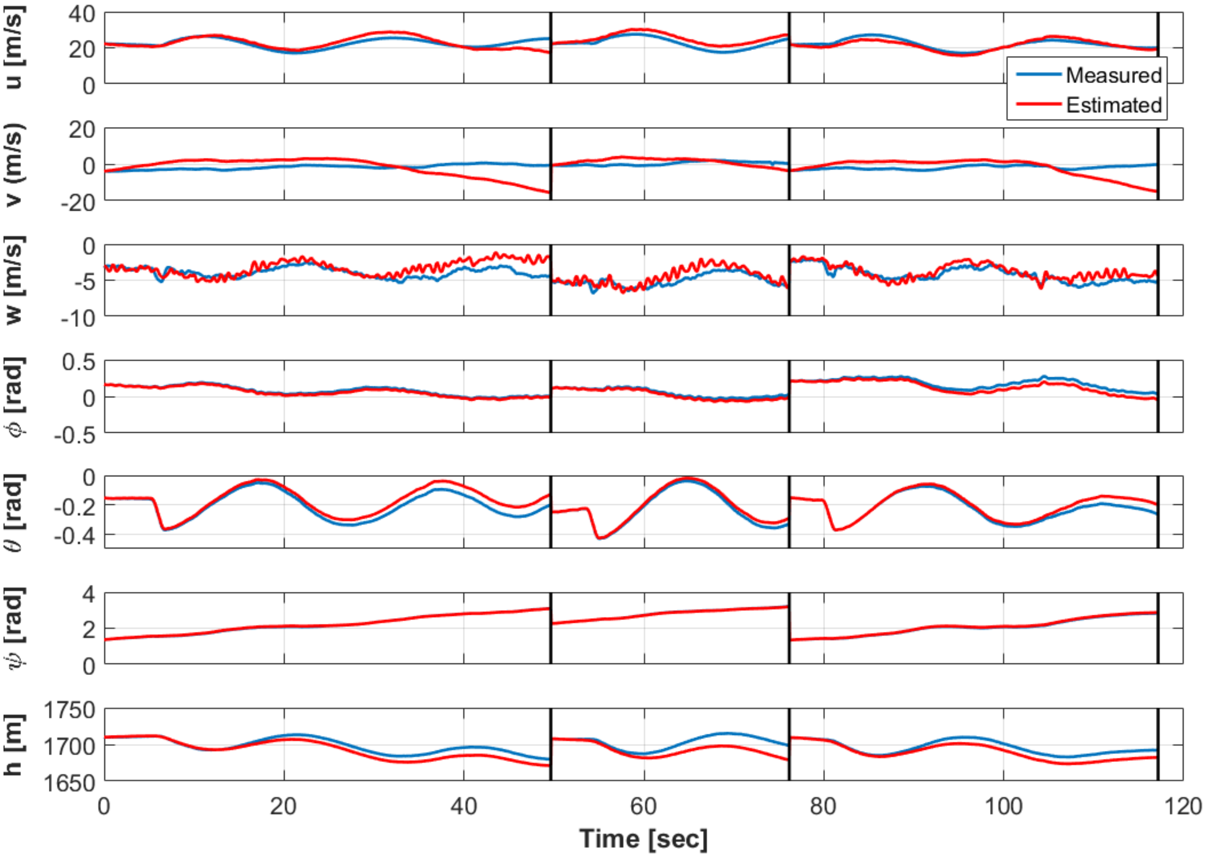

Figure 4.4: Measured longitudinal and lateral states and states generated from the integration of the 6DOF equations of motion with corrected accelerations: Validation Set

Table 4.6: Orientation of IMU sensor w.r.t. body axes: Validation Set

Orientation	Maneuver 1	Maneuver 2	Maneuver 3
ϕ’	-8.22	-9.79	-4.04
θ’	-6.95	-5.87	-8.12
ψ’	-9.74	10.01	-9.03

Once, the accelerations were corrected for the misalignment errors, they were then used in flight path reconstruction where the biases in the linear accelerations and the angular rates were estimated for the flight data belonging to the validation set. The comparison of the recorded states and the states estimated in the flight path reconstruction is presented in Fig. 4.5. As previous cases, it is observed that except the lateral velocity all other states provide a good match. The values of the biases estimated for linear accelerations and the angular rates for different maneuvers of the validation set are expressed in Table 4.7. The statistical measures for the estimated states using the flight path reconstruction are provided in Table 4.8

Once, the states have been reoriented and corrected for the estimated biases in linear

Table 4.7: Estimated measurement biases for each maneuver: Validation Set

Orientation	Maneuver 1	Maneuver 2	Maneuver 3
b_{ax}	0.251	0.297	0.035
b_{ay}	0.195	0.309	0.446
b_{az}	-0.048	-0.01003	-0.053
b_p	-0.001	-0.0016	-0.0028
b_q	9.38×10^{-04}	7.17×10^{-04}	-1.9×10^{-05}
b_r	2.04×10^{-04}	-3.5×10^{-04}	0.00114

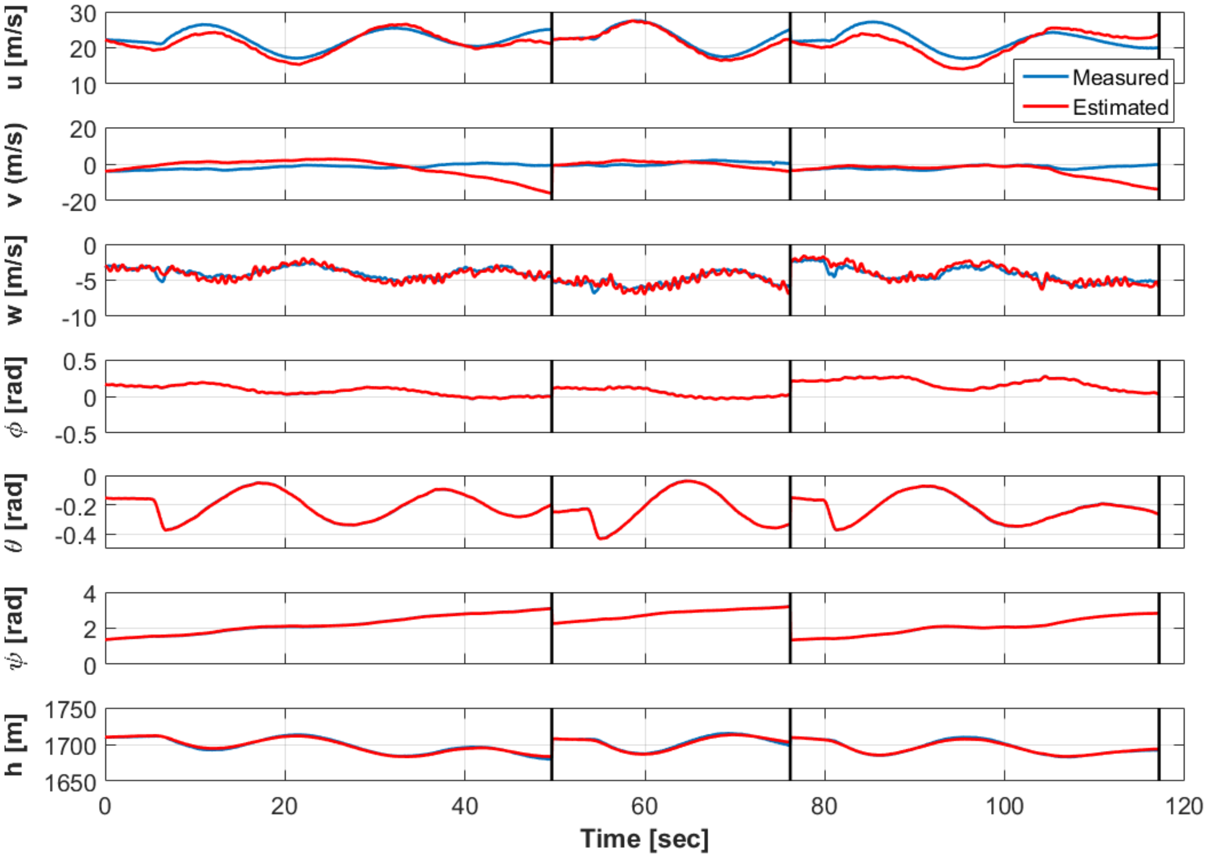

Figure 4.5: Measured longitudinal and lateral states and states generated from the integration of the 6DOF equations of motion with estimated biases added: Validation Set

Table 4.8: Statistical measures of the reconstructed states: Validation Set

Measure	u	v	w	ϕ	θ	ψ	h
GOF	0.567	-9.288	0.745	0.999	0.999	0.999	0.98
TIC	0.0405	0.685	0.054	0.0054	0.0028	0.00204	0.0004

accelerations and the angular rates for the validation set, the longitudinal force and moment derivatives were not calculated again. Instead, the already computed force and moment derivatives in the identification set were used to generate the dynamic model of the aircraft using the linear expressions where the states in this case were the states recorded for the maneuvers in the validation set. A comparison has been made between the forces generated using the force and moment derivatives estimated in the identification set and the ones reconstructed from the measurements as shown in Fig. 4.6. It can be seen that the estimated model using the system identification approach depicts a good match with the one which is reconstructed from the measurements.

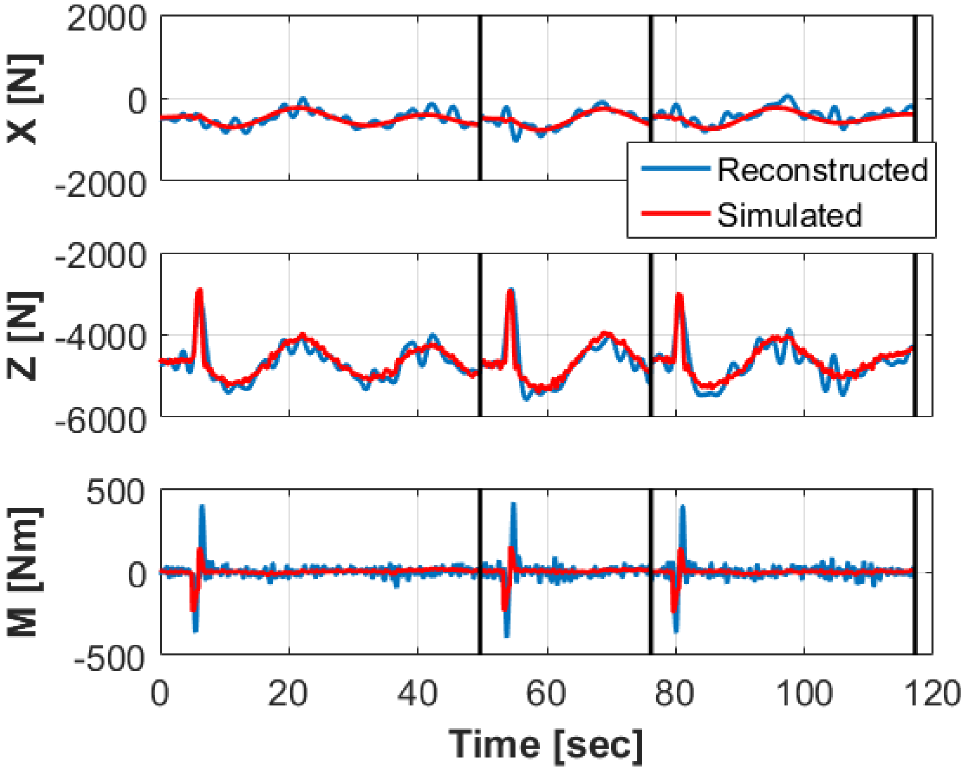

Figure 4.6: Reconstructed forces and moments, and forces and moments from linear regression: Validation Set

The obtained aerodynamic model was validated using various statistical measures. Two different measures R^2 and NRMSE (from Section 2.3.1) were applied on the generated longitudinal forces and moments in order to validate the model identified using the system identification approach. It can be seen from Table 4.9 that the model obtained depict a good match specially for the NRMSE values it can be seen the values are close to 0. The validity of the estimated biases and the estimation of the longitudinal forces and moments have been checked using various statistical measures and also using a different set of flight data which was not used for the identification approach. Hence, it can be assumed that the system identification approach provides an adequate flight dynamic model of the aircraft to proceed for the control design.

Table 4.9: Statistical measures of the longitudinal force and moments using Two step method: Validation Set

Measure	X	Z	M
R^2	0.60286	0.77576	0.31477
NRMSE	0.11124	0.081803	0.0058518

4.2.3 Forward Simulation

To further prove the validity of the aerodynamic model estimation from longitudinal states of the aircraft namely u, w, q and θ are reconstructed using the aircraft equations of motion. Initial conditions are chosen as trim states. The longitudinal states measurements are compared to the trajectories obtained from interpreting the aircraft equations of motion using the estimated aerodynamic force and moment as shown in Fig. 4.7. It can be seen that the estimated states provide a match in the period but amplitudes provide a poor match which is due the quality of flight data. The reasons for not a precise match could be due to not considering the engine dynamics in the identification. Moreover, the vertical velocity w shows an overall insufficient estimates due to the issues in heading sensor measurements using the given system identification approach.

It is quite hard to obtain a precise match for the state level validation. It can be concluded that the model identified is not ideal but is adequate for the control design.It can be guaranteed that the system identification approach is good because the approach was also tested for the flight experiments from another aircraft and they provided a precise aircraft model (See Appendix A).

In Fig. 4.8, the sensor measurements of the longitudinal states are compared to the trajectories obtained from solving the aircraft equations of motion using the estimated force and moment for the validation set. Table 4.10 and Table 4.11 provide the statistical measures for the states obtained using the force and moment estimations in the aircraft equations of motion. The GOF and TIC values are high for the vertical velocity again because of the instabilities caused by the heading measurements.

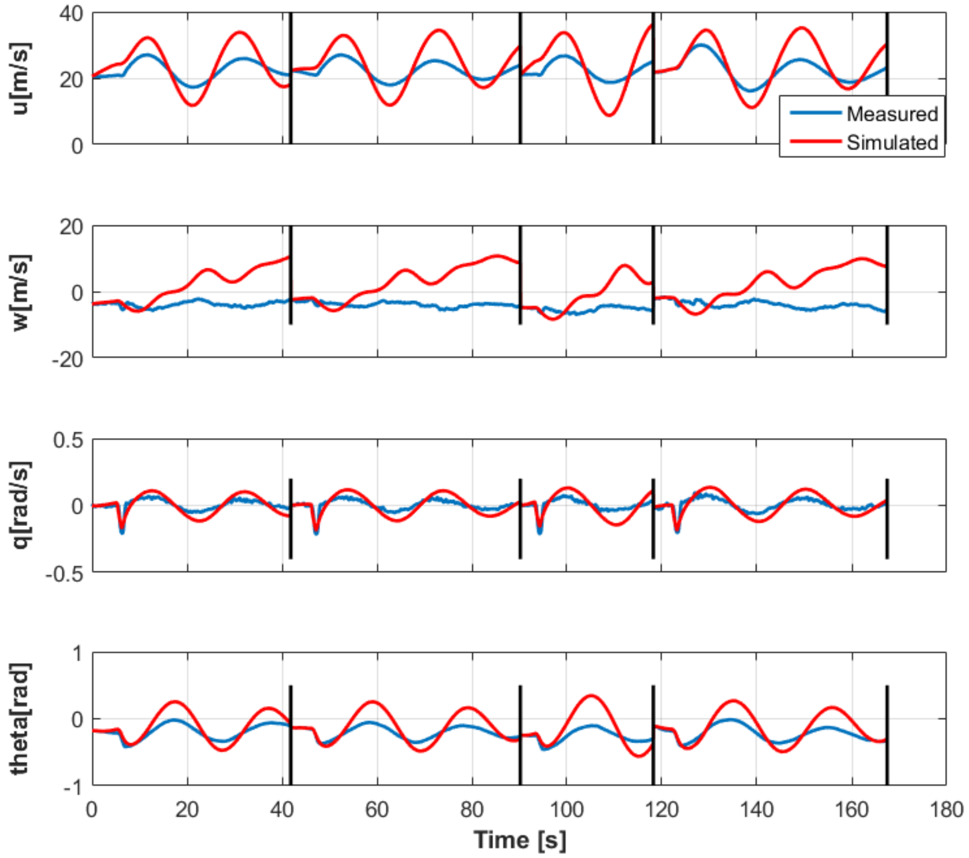

Figure 4.7: Validation of Estimated model using aircraft equations of motion: Identification Set

Table 4.10: Statistical measures of the states obtained using Two step method: Identification Set

Measure	u	w	q	θ
GOF	-1.556	-60.634	-0.07206	-1.659
TIC	0.0984	0.8099	0.3746	0.3372

Table 4.11: Statistical measures of the states obtained using Two step method: Validation Set

Measure	u	w	q	θ
GOF	-1.648	-55.276	-0.00679	-2.4185
TIC	0.0936	0.764	0.3708	0.3564

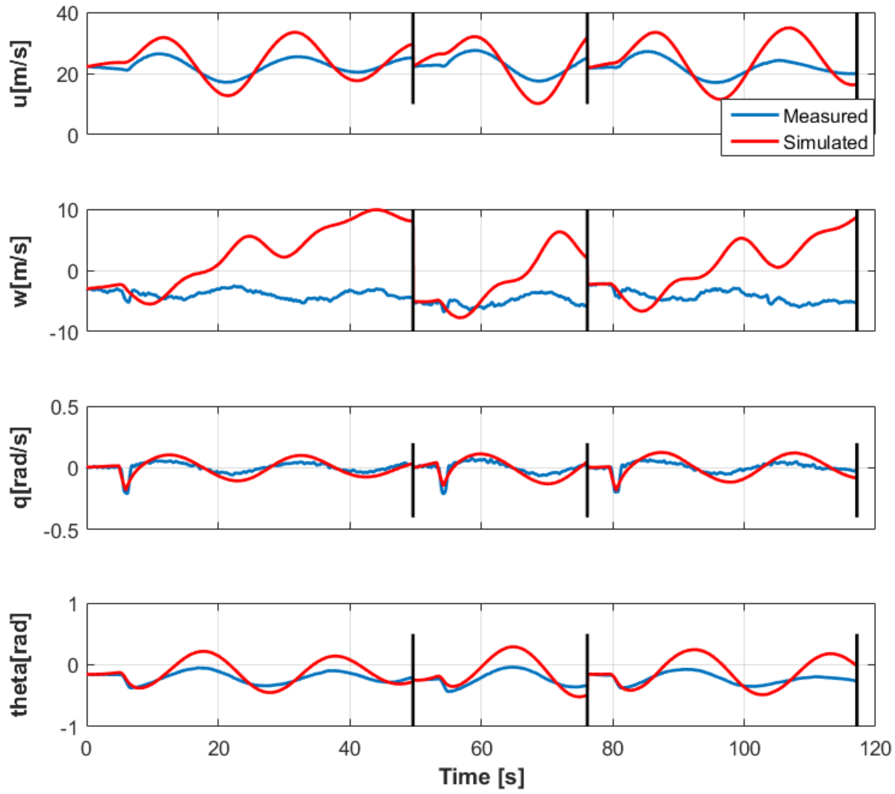

Figure 4.8: Validation of Estimated model using aircraft equations of motion: Validation Set

4.3 Control Design

4.3.1 Initial Control Design

As an initial control design and starting point for the optimization-based tuning procedure, the controller gains were tuned in flight using the Ziegler Nichols method. The response of the control design focusing the longitudinal model was tested by providing some step inputs in airspeed, altitude and course angle. The response obtained for the airspeed, altitude and the course angle for a single simulation are shown in Fig. 4.9, Fig. 4.10 and Fig. 4.11. It can be seen that there is a coupling effect seen in the airspeed plot at 40 seconds when there is step in altitude and at 66 seconds when there is a step in the course angle. The same observation can be seen in the altitude and the course angle plots in Fig. 4.10 and Fig. 4.11 respectively. This coupling is natural and gets settled soon, which shows the reliability of the control design.

4.3.2 Stability of the Control system

The stability analysis of the control design is performed by plotting bode diagram considering the transfer function between airspeed and the desired airspeed. A comparison has been made

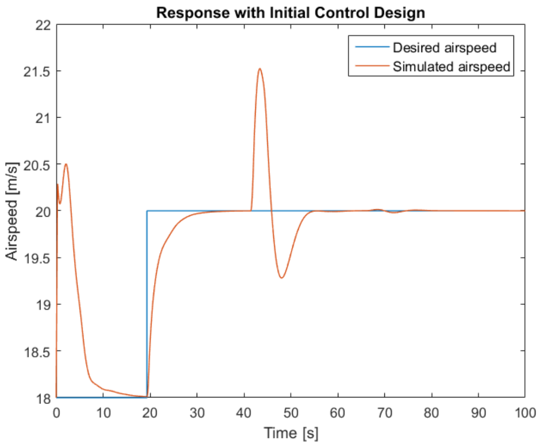

Figure 4.9: Response for Airspeed

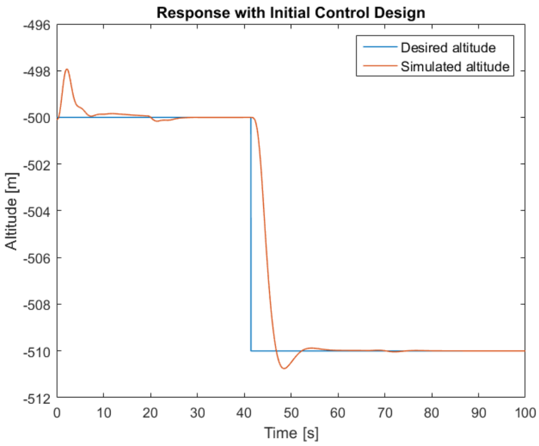

Figure 4.10: Response for Altitude

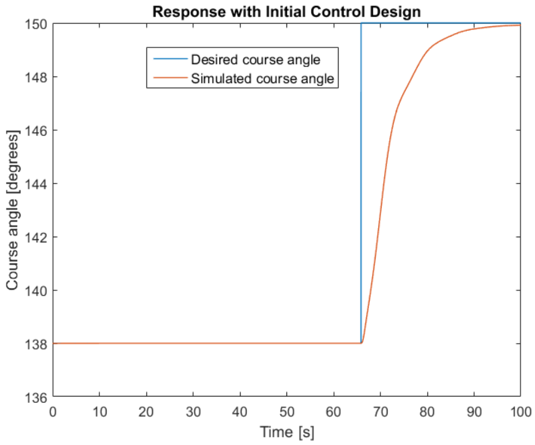

Figure 4.11: Response for course angle

for the frequency domain analysis using the bode diagram between the system with initial control design and the one with the optimization based control design.

It can be seen in Fig. 4.12 and Fig. 4.13 that the gain and phase margins both are positive, making the system stable. In Fig. 4.12, the gain margin is 8.73 dB and phase margin is 177 degrees. However, in Fig. 4.13 the increase in the gain margin (becomes 9.78 dB) and phase margins (becomes 179 degrees) reveals that the performance of the system improves with the optimization based control design.

The performance of the control design is also examined by its time response to test the optimization based control design. Several characteristics of the step response are analysed for the control design in order to prove its validity for the stratospheric flight mission. As it can be observed in Fig. 4.14 and Fig. 4.15, there is no overshoot for this chosen transfer function between the desired airspeed (the setpoint commanded) and the simulated airspeed, hence the setting time was selected as the main measure to compare the response. The settling time with

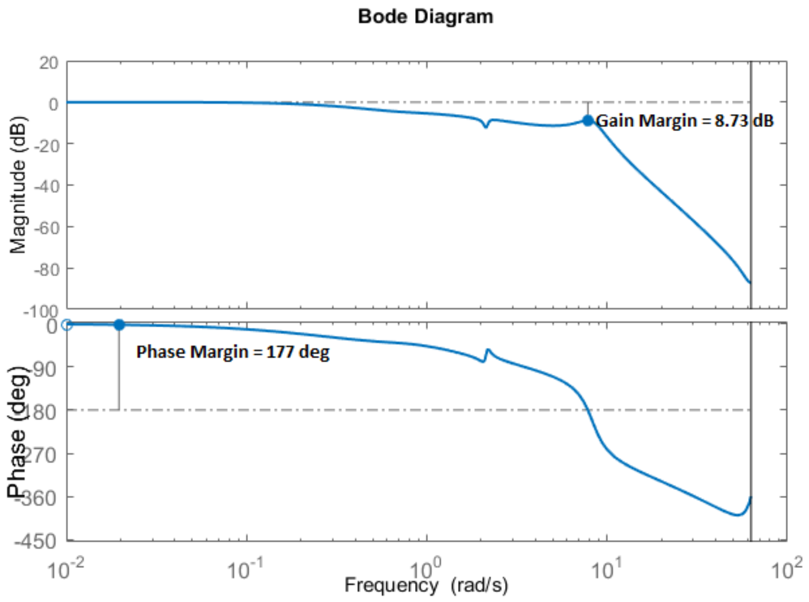

Figure 4.12: Bode Diagram for the system with Initial Control Design

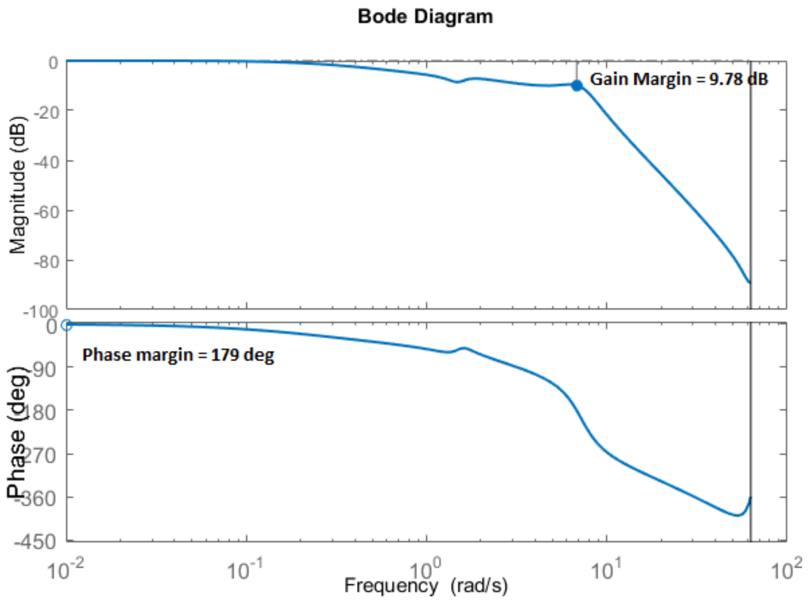

Figure 4.13: Bode Diagram for the system with Optimization-based Control Design

the initial control design was 17.6 seconds which has decreased (became 14 seconds) with the optimization based control design which is a demonstration of the reliability of the optimization based control design.

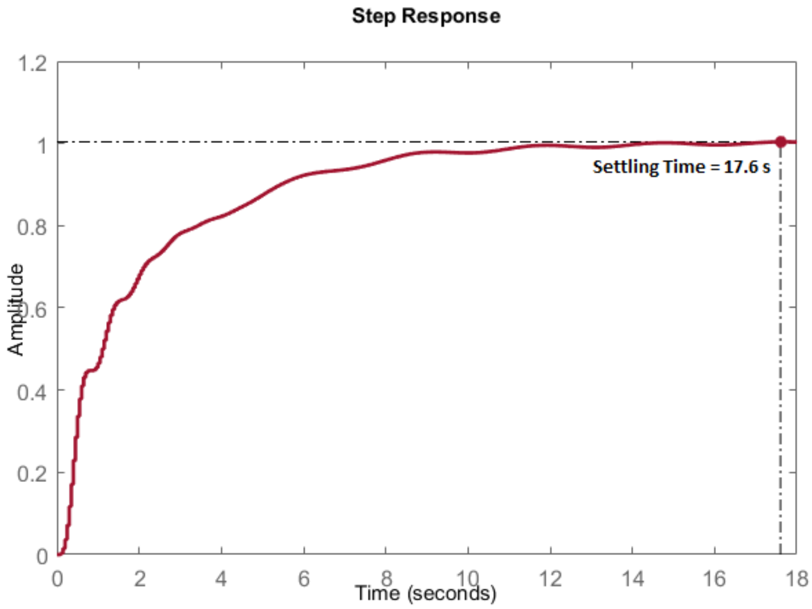

Figure 4.14: Step response for airspeed with Initial Control Design

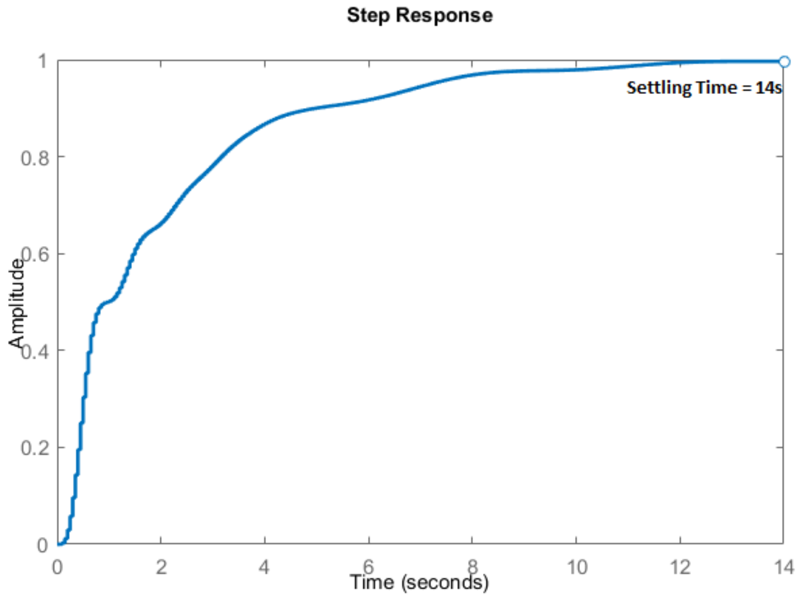

Figure 4.15: Step response for airspeed with Optimization-based Control Design

4.3.3 Robustness Analysis

Monte Carlo experiments have been used to assess the robustness of the control design. The uncertainties are provided to analyse the robustness of the control design when the system is at trim point. The control design is considered robust only if the system returns to its normal condition (trim point here) once the disturbance has settled down. [31] The outputs of interest are the performance measures considered during the definition of objectives and they can vary according to the requirements based on the application in such experiments.

In the first case, a gust disturbance is provided to the system. This gust disturbance is a combination of a crosswind and a tailwind. This crosswind and tailwind each are designed as a normal distribution with mean of 5 m/s and standard deviation of 0.06. Fig. 4.16 and Fig. 4.17 show an output signal for the designed gust disturbance from a Monte Carlo simulation, the ripples in the signals are because of the random inputs.

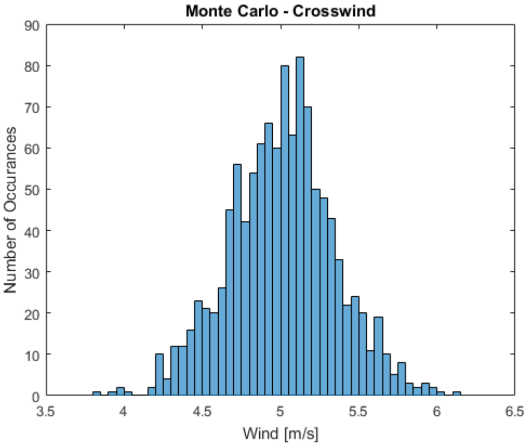

Figure 4.16: Distribution of Crosswind

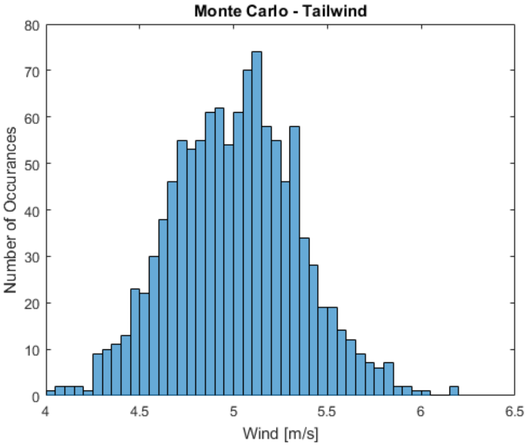

Figure 4.17: Distribution of Tailwind

The outputs observed in this test were mainly maximum overshoot and undershoot in the steady state and the settling time after providing the gust disturbance to the system. The initial overshoot in the airspeed is certainly due to the initial conditions not matching the trim and also due to the presence of the background wind. It can be observed in Fig. 4.18 from the time domain output from a Monte Carlo experiment. As the gust disturbance is provided after 50 seconds, there are sudden variations in the signals for airspeed signals. The reliability of the control design is proven from the fact that after a few seconds the system returns back to the normal trim condition. The Overshoot and undershoot corresponding the airspeed output signals are shown in Fig.4.19 and Fig.4.20. It can be noticed in all the following cases that the undershoot is greater than overshoot due to the reason that the gust disturbance is a tail wind.

Similar observations for overshoot and undershoot were made for the same gust experiments for altitude signals. It can be observed in Fig. 4.21 from the time domain output from a Monte Carlo experiment. As the gust disturbance is provided after 50 seconds, there are sudden variations in the signals for altitude signals just like airspeed. The reliability of the control design is proven from the fact that after a few seconds the system returns back to the normal trim condition. The Overshoot and undershoot corresponding the altitude output signals are shown in Fig. 4.22 and Fig. 4.23. Also, in the case of altitude, because the gust disturbance is

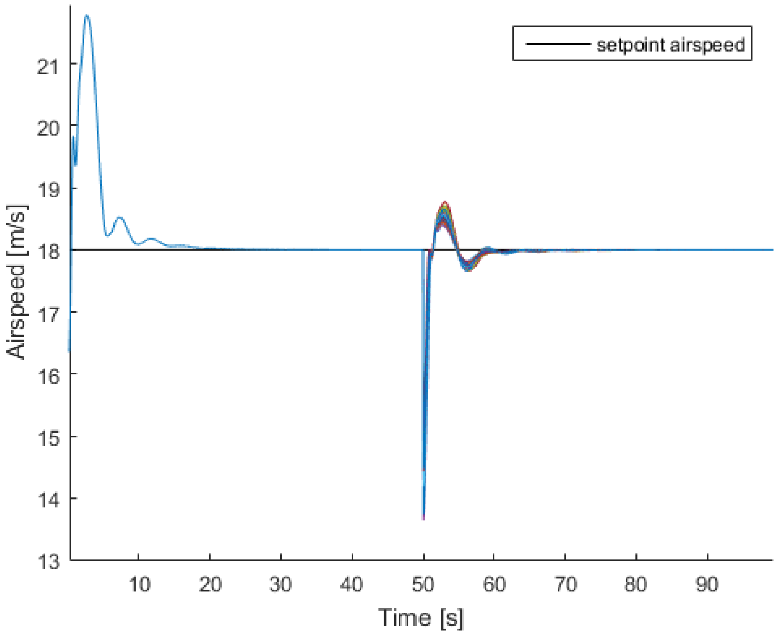

Figure 4.18: Airspeed output from a Monte Carlo experiment with gust disturbance

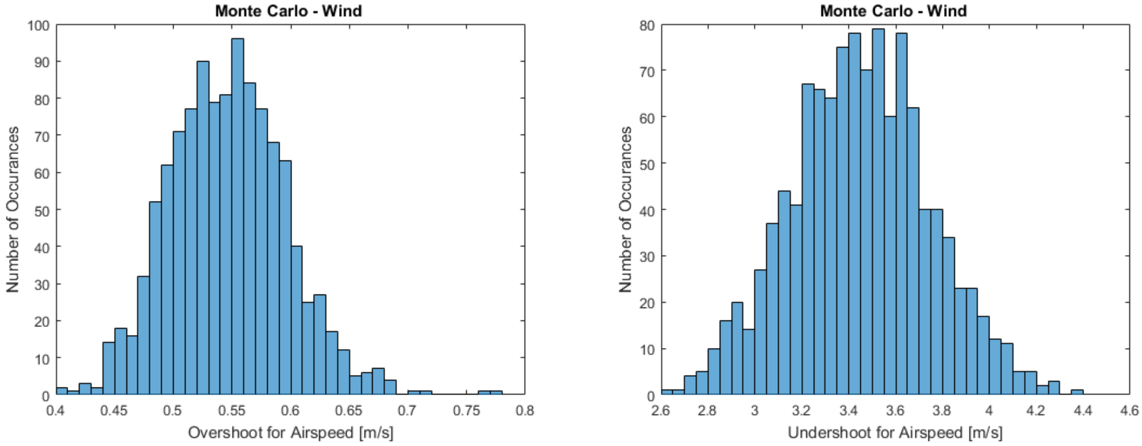

Figure 4.19: Overshoot in Airspeed

Figure 4.20: Undershoot in Airspeed

a tailwind, the value of of undershoots for various cases are greater than the overshoot values in the given Monte Carlo experiment which is also due to the definitions of overshoots and undershoots considered [32].

Another experiment was performed also to test for the internal model uncertainties along with the external gust disturbances using Monte Carlo experiments. In this case, along with the external gust disturbance, the identified longitudinal force and moment model parameters (from the system identification process) are also disturbed randomly in a defined range of 5% using Monte Carlo Simulations. The disturbance in the model parameters is designed as a normal distribution with mean at their identified values using the system identification process and a

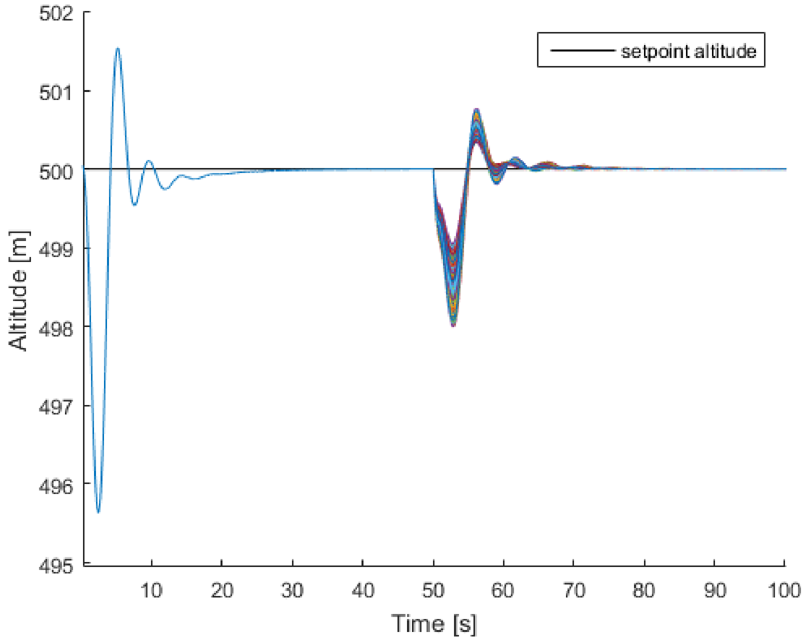

Figure 4.21: Altitude output from a Monte Carlo experiment with gust disturbance

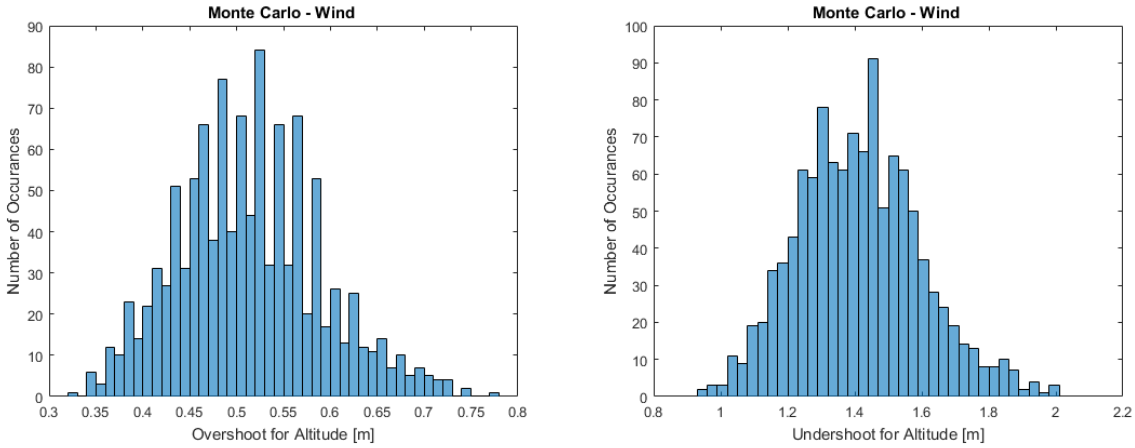

Figure 4.22: Overshoot in Altitude

Figure 4.23: Undershoot in Altitude

standard deviation of 0.01.

The outputs observed in this test were again maximum overshoot and undershoot in the steady state after providing the gust disturbance along with the model parameter variations. It can be observed in Fig. 4.24 from the time domain output from a Monte Carlo experiment. As the gust disturbance is provided after 50 seconds, there are sudden variations in the signals for airspeed signals also the magnitude of the variations becomes larger due to the fact that the model parameters are also being disturbed. Also, the reason for this could be the optimization based tuning was done for the nominal values of the parameters. In addition, as after a few seconds the system returns back to the normal trim condition, the control design is validated for

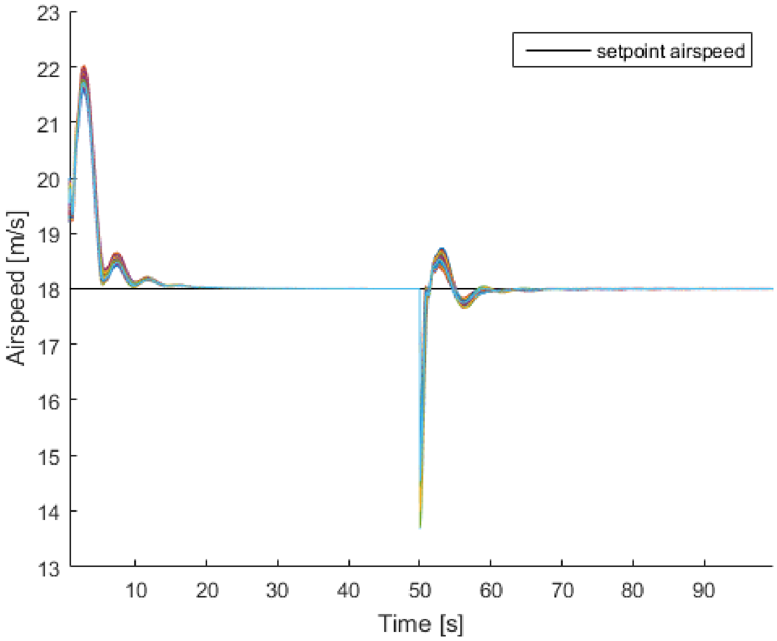

Figure 4.24: Airspeed output from a Monte Carlo experiment with gust disturbance and model parameter variations

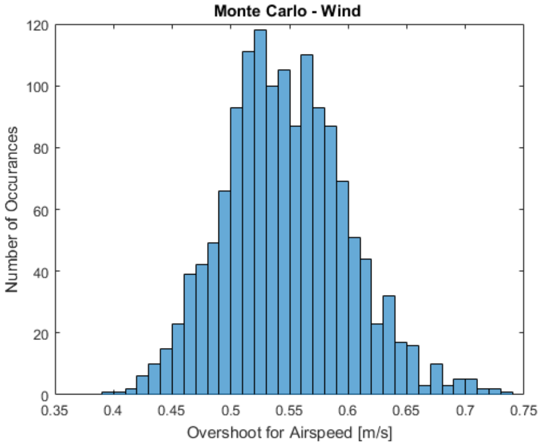

Figure 4.25: Overshoot in Airspeed

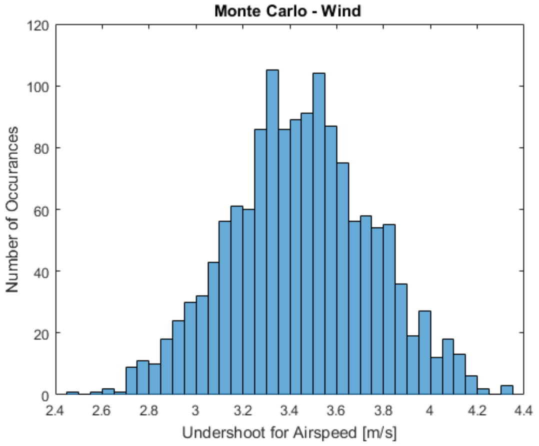

Figure 4.26: Undershoot in Airspeed

further strong disturbances. The overshoot and undershoot corresponding the airspeed output signals are shown in Fig.4.25 and Fig.4.26.

For these combination of gust disturbance and model parameter disturbance, the overshoot and undershoot were observed also for the altitude signals. As the system comes back the the normal conditions after the gust disturbance, its reliability is proven which can be observed in Fig. 4.27 from the time domain output from a Monte Carlo experiment. The Overshoot and undershoot corresponding the altitude output signals are shown in Fig.4.28 and Fig.4.29. It can be observed that the overshoot and undershoot have increased slightly than the previous case

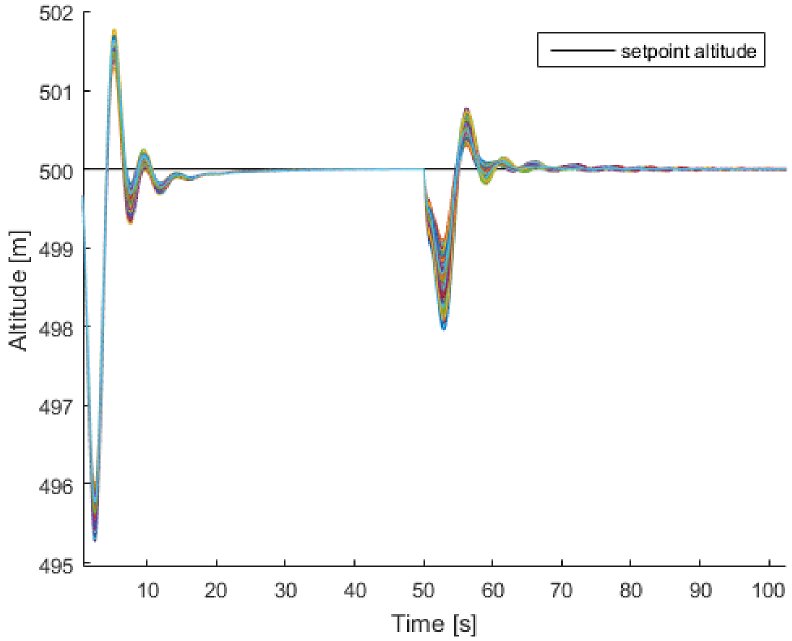

Figure 4.27: Altitude output from a Monte Carlo experiment with gust disturbance and model parameter variations

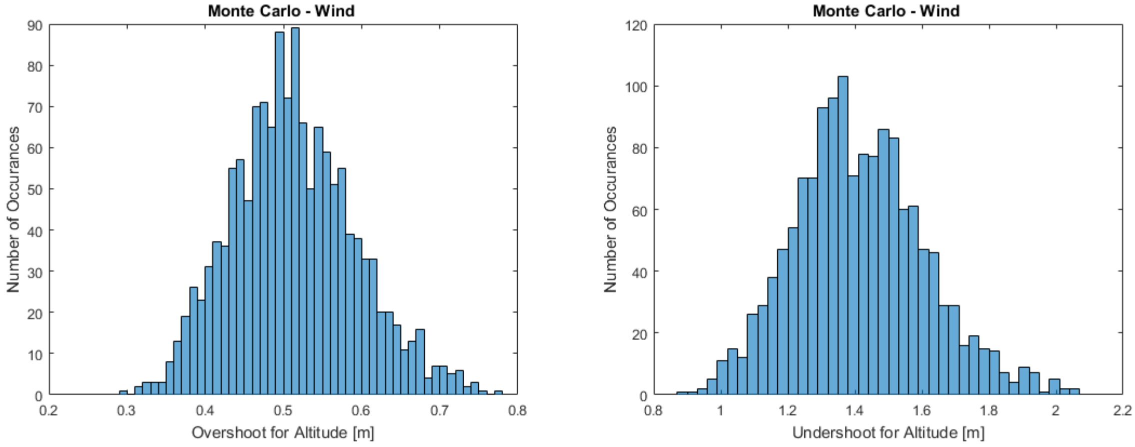

Figure 4.28: Overshoot in Altitude

Figure 4.29: Undershoot in Altitude

due to the fact there is an increase in the disturbance also in the longitudinal model parameters of the system. But the rise is not very large due to the fact the variations in the model parameters was done for a small range.

Conclusions and Future Perspectives

The system identification toolchain based on Two Step Method has been implemented for the aircraft-Elektra 2. A linear longitudinal flight dynamics model has been developed for Elektra 2. The identified model has been validated using various statistical measures. The recorded flight data was processed before using in the system identification process. The instrumentation biases in the linear accelerations and the angular rates have been identified as an output of the first step, flight path reconstruction. The aircraft states are corrected for these biases and then used in the second step to identify the longitudinal force and moment derivatives. The output of this system identification process is a longitudinal aircraft model which is further validated before being used in the control design.

Various statistical measures have been used to prove the reliability of the identified model by performing a residual analysis. The identified force and moment derivatives have been checked on a different set of flight data to validate the implemented algorithm. Moreover, a forward simulation is performed for a state level validation. It can be noted that the model obtained is not certainly good, but the system identification toolchain is tested for other flight experiment for different aircraft (results provided in Appendix A).

An optimization based control design has been presented which indicates a better performance and robustness than the earlier PID tuner based control design. The further validation for controller synthesis is done by performing a frequency domain analysis and a robustness analysis using Monte-Carlo simulations providing a wind disturbance and model parameter variations.

As a future development, identification of a lateral model can also be included in the system identification process. As an additional step, nonlinear engine dynamics can be included in the identification process. As an initial step, the identification framework has been developed which can now be used to further develop a global identification technique to develop global simulation models[13]. Further, for the control design, robust control laws can be used to design the controller to make it more robust in cases of unknown uncertainties even for the higher altitudes during the autonomous stratospheric flights.

Bibliography

[1] Elektrasolar gmbh website kernel description. `https://www.elektra-solar.com/`. Accessed: 2019-07-5.

[2] Mathworks website kernel description. `https://de.mathworks.com/help/control/ref/stepinfo.html`. Accessed: 2019-08-5.

[3] Wilson Marques. Analysis and comparison of cooperative control architectures for landing a small fixed-wing aircraft on a mobile platform, 2018.

[4] Tin Muskardin, Georg Balmer, Sven Wlach, Konstantin Kondak, Maximilian Laiacker, and Anibal Ollero. Landing of a fixed-wing uav on a mobile ground vehicle. In *2016 IEEE International Conference on Robotics and Automation (ICRA)*, pages 1237–1242. IEEE, 2016.

[5] Tin Muskardin, Georg Balmer, Linnea Persson, Sven Wlach, Maximilian Laiacker, Anibal Ollero, and Konstantin Kondak. A novel landing system to increase payload capacity and operational availability of high altitude long endurance uavs. *Journal of Intelligent & Robotic Systems*, 88(2-4):597–618, 2017.

[6] Harold Youngren Mark Drela. Athena Vortex Lattice kernel description. `http://web.mit.edu/drela/Public/web/avl/`. Accessed: 2019-07-5.

[7] Thomas Lombaerts. Aerodynamic model identification of frauke uav. In *AIAA Atmospheric Flight Mechanics Conference*, page 4512, 2012.

[8] David J Grymin and Mazen Farhood. Two-step system identification and trajectory tracking control of a small fixed-wing uav. *Journal of Intelligent & Robotic Systems*, 83(1):105–131, 2016.

[9] Ravindra V Jategaonkar. *Flight vehicle system identification: A time-domain methodology*. American Institute of Aeronautics and Astronautics, Inc., 2015.

[10] Joao Oliveira, QP Chu, JA Mulder, HMNK Balini, and WGM Vos. Output error method and two step method for aerodynamic model identification. In *AIAA Guidance, Navigation, and Control Conference and Exhibit*, page 6440, 2005.

[11] Vladislav Klein and Eugene A Morelli. *Aircraft system identification: theory and practice*. American Institute of Aeronautics and Astronautics Reston, VA, 2006.

[12] David J Grymin. *Two-step system identification and primitive-based motion planning for control of small unmanned aerial vehicles*. PhD thesis, Virginia Tech, 2013.

[13] Jongseok Lee. *High Fidelity Modelling for High Altitude Long Endurance Solar Powered Aircraft*. PhD thesis, ETH Zürich, 2017.

[14] HL Stalford. High-alpha aerodynamic model identification of t-2c aircraft using the ebm method. *Journal of Aircraft*, 18(10):801–809, 1981.

[15] H Stalford. High-alpha aerodynamic model identification of the t-2c aircraft using the ebm system identification method. In *18th Aerospace Sciences Meeting*, page 172, 1980.

[16] RJ Evans, GC Goodwin, RA Feik, C Martin, and R Lozano-Leal. Aircraft flight data compatibility checking using maximum likelihood and extended kalman filter estimation. *IFAC Proceedings Volumes*, 18(5):487–492, 1985.

[17] CA Martin, RA Feik, et al. Estimation of aircraft dynamic states and instrument systematic errors from flight test measurements. In *Second Conference on Control Engineering 1982: Merging of Technology and Theory to Solve Industrial Automation Problems; Preprints of Papers*, page 174. Institution of Engineers, Australia, 1982.

[18] Fredrik Gustafsson. Determining the initial states in forward-backward filtering. *IEEE Transactions on signal processing*, 44(4):988–992, 1996.

[19] Peter G Hamel and Ravindra V Jategaonkar. Evolution of flight vehicle system identification. *Journal of aircraft*, 33(1):9–28, 1996.

[20] Eugene A Morelli and Vladislav Klein. Application of system identification to aircraft at nasa langley research center. *Journal of Aircraft*, 42(1):12–25, 2005.

[21] Jorge J Moré. The levenberg-marquardt algorithm: implementation and theory. In *Numerical analysis*, pages 105–116. Springer, 1978.

[22] JA Mulder, QP Chu, JK Sridhar, JH Breeman, and M Laban. Non-linear aircraft flight path reconstruction review and new advances. *Progress in Aerospace Sciences*, 35(7):673–726, 1999.

[23] Alvin C Rencher. A review of “methods of multivariate analysis, ”, 2005.

[24] Michael V Cook. *Flight dynamics principles: a linear systems approach to aircraft stability and control*. Butterworth-Heinemann, 2012.

[25] Karl Johan Aström and Richard M Murray. *Feedback systems: an introduction for scientists and engineers*. Princeton university press, 2010.

[26] Karl Johan Åström and Tore Hägglund. *PID controllers: theory, design, and tuning*, volume 2. Instrument society of America Research Triangle Park, NC, 1995.

[27] Jeffrey C Lagarias, James A Reeds, Margaret H Wright, and Paul E Wright. Convergence properties of the nelder–mead simplex method in low dimensions. *SIAM Journal on optimization*, 9(1):112–147, 1998.

[28] Swarup BhattacharjeeJ. Frequency domain analysis of control systems, 2015.

[29] William Bolton. *Instrumentation and control systems*. Newnes, 2015.

[30] Klee Harold and Allen Randal. Simulation of dynamical systems with matlab and simulink (2011).

[31] Sigurd Skogestad and Ian Postlethwaite. *Multivariable feedback control: analysis and design*, volume 2. Wiley New York, 2007.

[32] Benjamin C Kuo and Farid Golnaraghi. *Automatic control systems*, volume 9. Prentice-Hall Englewood Cliffs, NJ, 1995.

[33] Andreas Klöckner. Geometry based flight dynamics modelling of unmanned airplanes. In *AIAA Modeling and Simulation Technologies (MST) Conference*, page 5154, 2013.

[34] John H Blakelock. *Automatic control of aircraft and missiles*. John Wiley & Sons, 1991.

[35] Georg Robert Balmer. Modelling and control of a fixed-wing uav for landings on mobile landing platforms, 2015.

Appendix A

System Identification Toolchain & Application to Elektra 1

A.1 Toolchain

The system identification tool chain contains following steps.

1. A priori model computation and Input design (see Table A.3).
2. Flight test experiments and Data extraction and pre-processing (see Table 3.2).
3. Identification of IMU orientation (see Table 3.5)
4. Data consistency check or reconstruction of path (see table 3.3).
5. Aerodynamic model identification (see Table 3.2) and validation (see Table 3.5)

A priori model computation is based on AVL software. [33]. A linear state space representation containing aerodynamic derivatives is obtained using the MATLAB's linmod function. The flight test experiments are performed according to the inputs designed suitable for the identification process. All other steps are provided in the following section.

1. Selection of Maneuver

Table A.1: Designing the Input

m-file	Remarks
Designing_Inputs_e2.m	Outputs the input signals and their energy spectrum. The time step and magnitude of the input signals must be selected to maximize the information on specific parameters.

2. Data Extraction and Pre-processing

Table A.2: Steps for Data Extraction and Pre-processing

m-file	Remarks
Import_e2.m	Imports raw data from the original folder, separate the desired signals in the time segments when the maneuvers were executed; interpolates the servo data to get the deflections in the control surfaces.
Processing_e2.m	All the duplicates are removed in this script. As the sampling rate varies for different data, all the signals are interpolates to be in the same sampling frequency (50 Hz) and the time reference (the time vector is now the same for all signals). The GPS data is converted from NED to body frame. All the signals are resampled to the final sampling rate used in the identification i.e. 20Hz.
Corrections_e2.m	Conversions from degrees to radians are done. Outliers are removed. Data is isolated for each maneuver and portioned into identification and validation sets. The data is saved under following names "DATA_ALL_ID_E2.mat" (for the identification set) and "DATA_ALL_VAL_E2.mat (for the validation set).

3. Two Step Method and Validation

Table A.3: Steps of the Two Step Method and Validation of the Model

m-file	Remarks
Main_oem.m	Implementation of Two-step method. Input to the file is "DATA_ALL_ID_E2.mat" (identification set) and "DATA_ALL_VAL_E2.mat (validation set). The script contains different cases for different steps of the identification process.

m-file	Remarks
	(a) Plots the comparison between measured and simulated responses with bias corrections for the longitudinal states. (b) Plots the comparison between force and moment computed from direction substitution in the equation of motion and Two-step method. (c)Does residual analysis, provides values of Goodness of Fit (GOF) and Theil's Inequality Coefficient (TIC).
mDefCase19.m	This case corresponds to Step 0 (for the identification set), to identify the orientation of the accelerometer data due to misalignment. The input to this file is "DATA_ALL_ID_E2.mat" (for the identification set) and the output is saved in a file 'angles_DataCompatibility_ID.mat' which gives the orientation of accelerometer with respect to CG.
mDefCase22.m	This case corresponds to Step 1 (Data Compatibility check for the identification set), to identify the biases in linear accelerations and angular rates. The input to this file is "DATA_ALL_ID_E2.mat" (for the Identification set). and the output is the vector containing biases in linear and angular accelerations which is saved as "biases_DataCompatibility_ID.mat"
mDefCase23.m	This case corresponds to Step 2 (for the identification set), to identify the longitudinal forces and moments. The input to this file is "DATA_ALL_ID_E2.mat" and "biases_DataCompatibility_ID.mat" the output is the vector containing longitudinal forces and moments which is saved as " longitudinal_forces_moments_ID2" and "results_step2_ID2"
mDefCase10.m	This case corresponds for a forward simulation of rigid body equations of motion. (for the identification set). The input to file is "DATA_ALL_ID_E2.mat" and longitudinal_forces_moments_ID2" and "results_step2_ID2".

m-file	Remarks
	With initial states from the measurements as its initial conditions and time histories of measured control inputs, the script computes the time histories of aircraft states, which is being compared to measured time histories of aircraft states for validation.
mDefCase20.m	This case corresponds to Step 0 (for the validation set), to identify the orientation of the accelerometer data due to misalignment. The input to this file is “DATA_ALL_VAL_E2.mat (for the validation set) and the the output is saved in a file ’angles_DataCompatibility_VAL.mat’ which gives the orientation of accelerometer with respect to CG.
mDefCase21.m	This case corresponds to Step 1 (Data Compatibility check for the validation set), to identify the biases in linear accelerations and angular rates. The input to this file is “DATA_ALL_VAL_E2.mat” (for the validation set). and the output is the vector containing biases in linear and angular accelerations which is saved as “biases_DataCompatibility_VAL.mat”
mDefCase24.m	This case corresponds to Step 2 (for the validation set). The input to this file is “DATA_ALL_VAL_E2.mat” and “biases_DataCompatibility_VAL.mat” and longitudinal_forces_moments_ID2” and “results_step2_ID2” in order to validate the longitudinal force and moment derivatives obtained from case 23.
mDefCase11.m	This case corresponds for a forward simulation of rigid body equations of motion. (for the validation set). The input to file is “DATA_ALL_VAL_E2.mat” and longitudinal_forces_moments_ID2” and “results_step2_ID2”. With initial states from the measurements as its initial conditions and time histories of measured control inputs, the script computes the time histories of aircraft states, which is being compared to measured time histories of aircraft states for validation.

A.2 Elektra 1

As the flight experiments involved various issues with the heading sensor measurement drifts and the mission planning change from a straight , the identification for Elektra 2 did not provide an ideal model. In order to justify the credibility of the presented system identification approach, the method was also tested for the flight experiments for a similar aircraft, Elektra 1. In this experiment, two phugoid maneuvers were chosen for performing the identification. Some of the results for which are provided in this section. It can be seen from Table A.4, the identified orientation of the IMU sensor is quite consistent in comparison to Elektra 2.

Table A.4: Orientation of IMU sensor w.r.t. body axes

Orientation	Maneuver 1	Maneuver 2
ϕ’	-1	-0.4
θ’	-0.5	0.45
ψ’	20.8	22.3

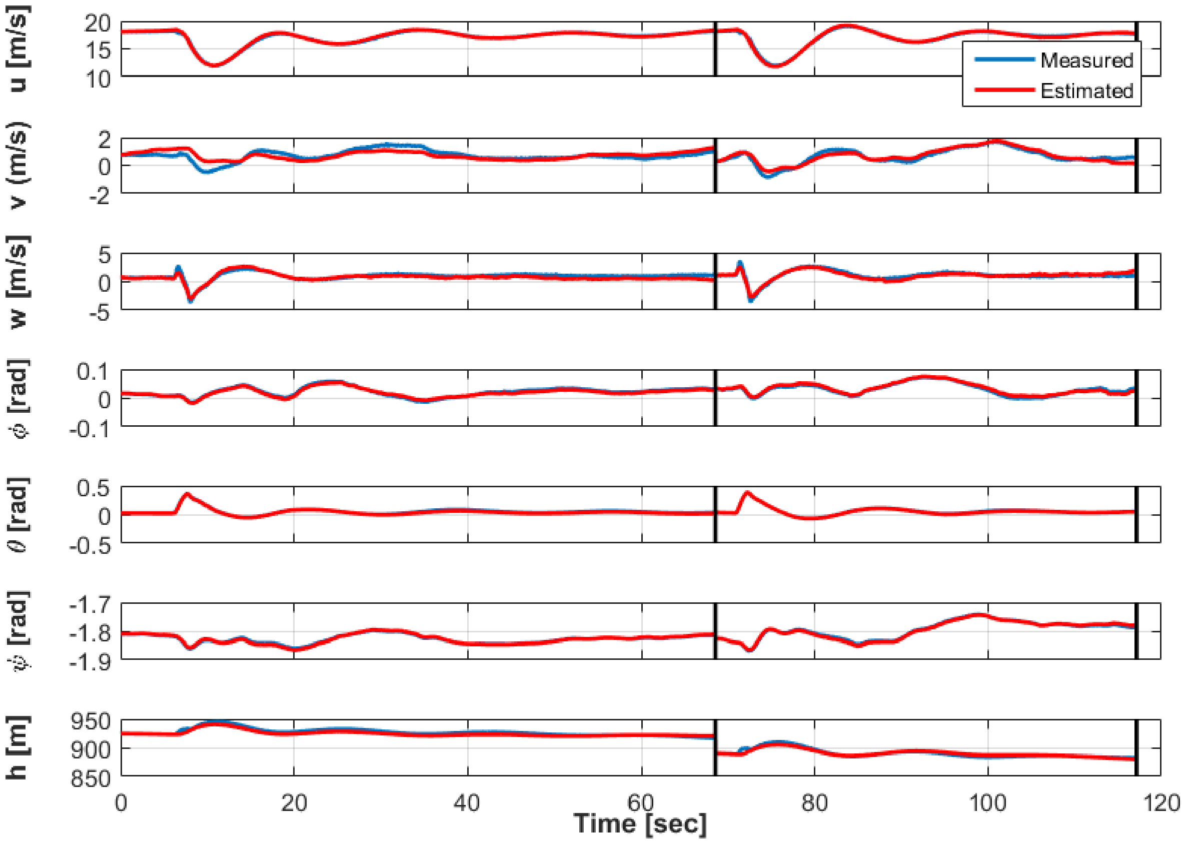

Figure A.1: Measured longitudinal and lateral states and states generated from the integration of the 6DOF equations of motion with estimated biases added: Identification Set

Table A.5 provides the biases estimated from the flight path reconstruction step of the identification process for Elektra 1. The order of the biases is comparatively small. It can be clearly seen from Fig. A.1 that the states provide a much better match which proves that the identification is better for the first step. The comparison for the reconstructed forces and

Table A.5: Estimated measurement biases for each maneuver

Orientation	Maneuver 1	Maneuver 2
b_{ax}	-0.0955	-0.0893
b_{ay}	-0.0149	-0.0153
b_{az}	-0.014	-0.0412
b_p	-7.23 $\times 10^{-05}$	5.304 $\times 10^{-05}$
b_q	-3.88 $\times 10^{-04}$	-5.46 $\times 10^{-04}$
b_r	-5.77 $\times 10^{-04}$	-0.001 $\times 10^{-04}$

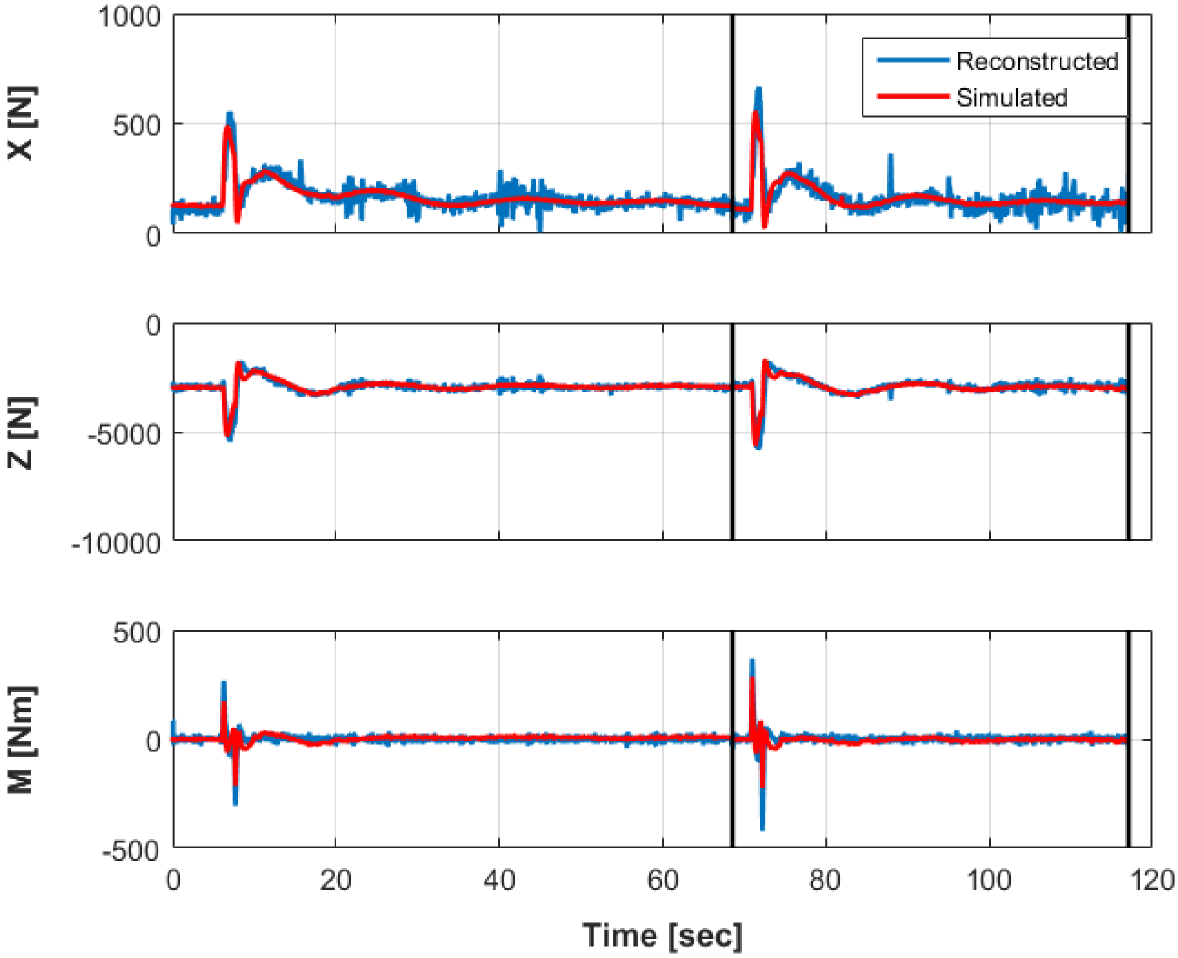

Figure A.2: Reconstructed forces and moments, and forces and moments from linear regression: Identification set

moments with the ones estimated from the second step of the Two Step method is presented in Fig. A.2. The forces and moment provides a better fit for Elektra 1 flight data.

Table A.6: Statistical measures of the reconstructed states using flight path reconstruction: Identification Set

Measure	u	v	w	ϕ	θ	ψ	h
GOF	0.9946	0.679	0.8093	0.9526	0.984	0.9905	0.9782
TIC	0.003	0.1612	0.1454	0.0671	0.0516	0.0007	0.0015

In order to validate the identification process, the statistical measures (2.3.1) were computed for the first and second step estimations. It can be seen from Table A.6 that GOF values being closer to 1 and the TIC values being small provide a good fit. Table A.7 indicates that the model identified is good. Also, a forward simulation was performed in order to do the state level validation. The GOF and TIC values for the states for this forward simulation are provided in Table A.8. It can be seen that the GOF values have improved in comparison to Elektra 2. Overall, it can be said that the identified model for Elektra 1 has been proved better than Elektra 2 which explains the credibility of the presented approach. The inaccuracy of the Elektra 2 model was certainly due the drifting heading measurements and also due to the circular motion performed during the flight which was supposed to be straight flight.

Table A.7: Statistical measures of the longitudinal force and moments using Two step method: Identification Set

Measure	X	Z	M
R^2	0.683	0.753	0.411
NRMSE	0.058	0.047	0.028

Table A.8: Statistical measures of the states obtained using Two step method: Identification Set

Measure	u	w	q	θ
GOF	0.8116	0.03	0.917	0.846
TIC	0.0193	0.2709	0.146	0.1538

Appendix B

Fundamental Control Design

To stabilize and make the aircraft follow commands, a control scheme is to be used. The primary goal of an autopilot system is to control position, velocity and attitude. For the autopilot design, a simplification is adopted where the longitudinal dynamics are considered decoupled from the lateral dynamics [34]. This assumption facilitates the control design without making a big effect for the model accuracy. The procedure used for the longitudinal control design is described in the following subsections.

B.1 Lateral Control Design

The lateral controller for Elektra Two consists of three cascaded SISO loops. The design begins with the innermost loop, which is a proportional controller with feedback of the roll rate p, which acts as a damping term for the attitude ϕ controller.

$$\delta_a = K_p(p_{des} - p) \tag{B.1}$$

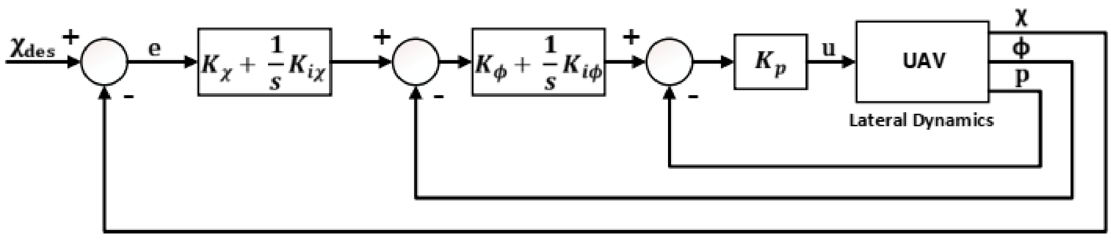
χ_{des}
+
-
e
$K_\chi + \frac{1}{s}K_{i\chi}$
+
-
$K_\phi + \frac{1}{s}K_{i\phi}$
+
-
K_p
u
UAV
Lateral Dynamics
χ
ϕ
p

Figure B.1: Lateral Autopilot Design [3]

The bank angle ϕ is controlled by a PI-controller, described by the Eq. B.2

$$p_{des} = \left(K_{\phi} + \frac{1}{s}K_{i\phi}\right) \cdot (\phi_{des} - \phi) \tag{B.2}$$

The course angle χ is controlled in the outermost loop. It was implemented as a PI controller with feedback of the course angle, which is measured with reference to the north. However, as the following inner loop described in Eq. B.2 expects a desired bank angle ϕ_{des}, it is necessary to calculate it according to Eq. B.4

$$\dot{\chi}_{des} = \left(K_{\chi} + \frac{1}{s}K_{i\chi}\right) \cdot (\chi_{des} - \chi) \tag{B.3}$$

$$\phi_{des} = \arctan(\frac{V_k \dot{\chi}_{des}}{g}) \tag{B.4}$$

B.2 Longitudinal Control Design

To initiate, the underdamped short-period mode was handled by adding a pitch rate feedback. Then, the inner loop for pitch angle was added. The final configuration of this inner loop for the pitch angle consists of a PI controller for θ. The control design for this inner loop is shown in Fig. B.2. The resulting controller is described by Eq. B.5.

$$\delta_e = -\left(K_{\theta} + \frac{K_{i\theta}}{s}\right)(\theta_{des} - \theta) - K_q q \tag{B.5}$$

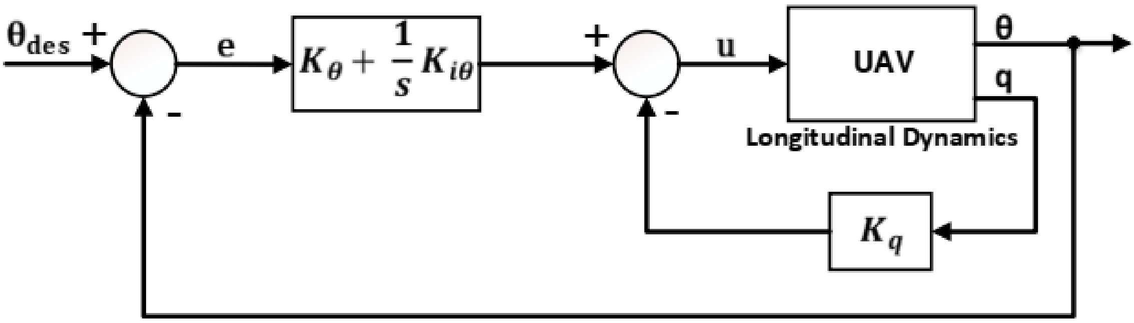

Figure B.2: Pitch angle inner loop [3]

The thrust loop for the longitudinal control design for Elektra 2 is shown in Fig. B.3). The thrust loop was also closed by a PI controller with a feed forward term which is described by the Eq. B.6. Due to the coupling between the airspeed and altitude commands in the longitudinal motion, it is not possible to design a successive loop control design for the longitudinal control as was presented for the lateral control.

$$\delta_t = -\left(K_\tau + \frac{K_{i\tau}}{s}\right)(\tau_{des} - \tau) - \delta_{tF}F \tag{B.6}$$

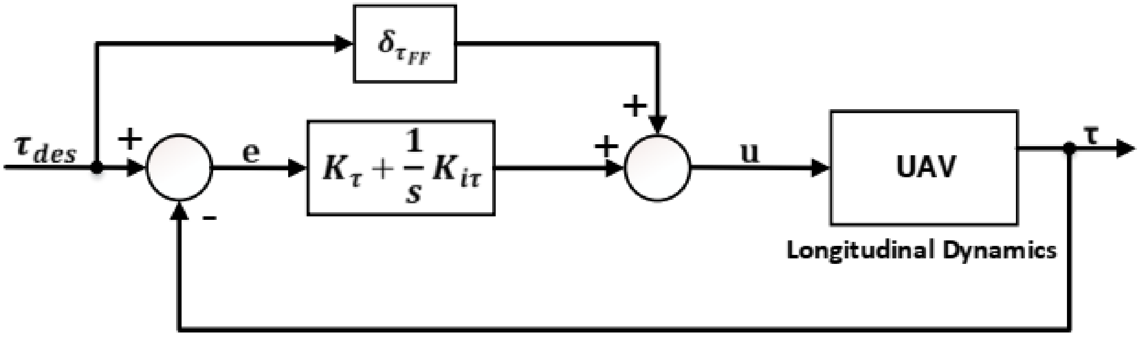

Figure B.3: Thrust inner loop [3]

B.3 TECS

With classical control methods, its quite hard to achieve the independent control of altitude and airspeed because of strong coupling. A way to reduce this coupling effect is to operate the system under different flight regimes, which generally results in an non-optimal performance. An alternative solution can be to use a different approach of controlling by using a method based on energy distribution; it distributes the total energy of the system between its kinematic and potential forms. This method is called Total Energy Control System (TECS), in this controller structure the throttle input is mainly responsible for adding energy into the system while the elevator control input distributes this energy accordingly. Various studies have been performed that provide a description of the implementation of TECS [35].

This TECS control design consists of an integrated control system using elevator and throttle in a coordinated manner so that the altitude and airspeed responses get decoupled. The dimensionless energy rates are used, which lead to the core algorithm provided in Eq. B.7 and

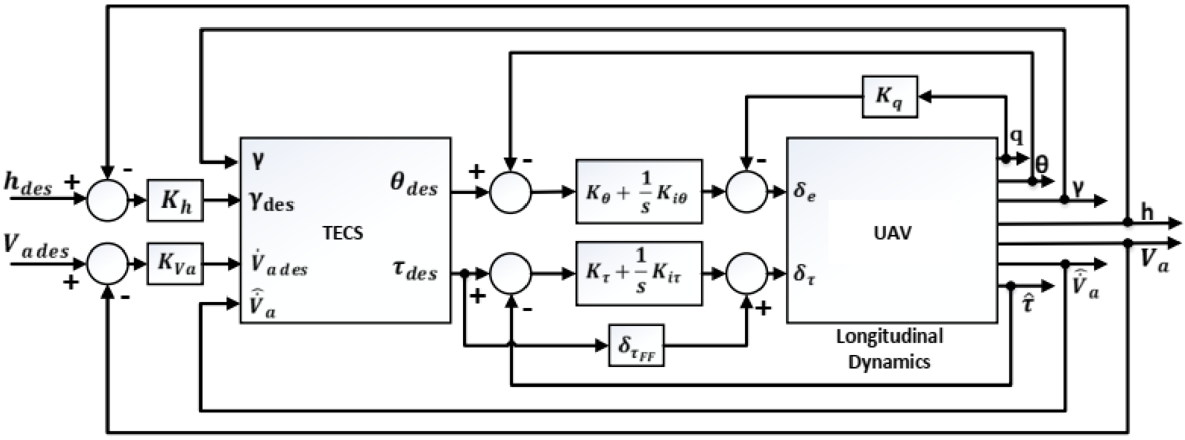
h_{des}
+
-
K_h
$V_{a\,des}$
+
-
K_{Va}
γ
γ_{des}
TECS
$\dot{V}_{a\,des}$
$\hat{V}_a$
θ_{des}
τ_{des}
+
-
+
-
$K_\theta + \frac{1}{s}K_{i\theta}$
$K_\tau + \frac{1}{s}K_{i\tau}$
$\delta_{\tau_{FF}}$
K_q
-
+
δ_e
δ_τ
UAV
Longitudinal Dynamics
q
θ
γ
h
V_a
$\hat{V}_a$
$\hat{\tau}$

Figure B.4: Longitudinal Autopilot Design [3]

Eq. B.8. The design of the whole longitudinal control design has been shown in Fig. B.4

$$\theta_{cmd} = -K_{EI}\frac{1}{s}\left(e_\gamma - \frac{e_{\dot{V}}}{g}\right) - K_{EP}\left(\gamma - \frac{\dot{V}}{g}\right) \tag{B.7}$$

$$\frac{F}{mg_{cmd}} = K_{TI}\frac{1}{s}\left(e_\gamma + \frac{e_{\dot{V}}}{g}\right) - K_{TP}\left(\gamma + \frac{\dot{V}}{g}\right) \tag{B.8}$$

where e_γ $e_{\dot{V}}$ represent the flight path angle and the acceleration errors respectively.